

Response to comments by referee 3

Specific comments:

The spatial and seasonal characteristics of mixing layer height (MLH) over northern China plain (NCP) were revealed by the authors using variety of measurements, primarily focusing on northern NCP and southern Hebei. The authors attempt to explain the different feature of MLH development between the two interested regions by examining observed wind shear, buoyancy and turbulent stability. In addition, this study pointed out that the MLH plays a key role in forming the heavy near-ground particular mater (PM) pollution besides emissions. The paper is well organized and the reasoning for MLH spatial variations and its association with air pollution is comprehensively discussed. I recommend to publish this paper in ACP journal after addressing following minor issues.

Comment 1:

For Fig. 6: What are the reasons for the difference in buoyancy term profiles between the site XT and BJ during winter, as shown in Fig. 6g? In addition, the absolute values of buoyancy term seem larger than that of shear term; does this mean the buoyancy term rather than the shear term is the dominant component in determining turbulent energy?

Response 1:

Thank you for your suggestion. As we described in section 2.4, the Gradient Richard

number (Ri) is the ratio of buoyancy term $\left(\frac{g}{\theta} \frac{\Delta \bar{\theta}}{\Delta z}\right)$ and shear term $\left(\left(\frac{\Delta \bar{u}}{\Delta z}\right)^2 + \left(\frac{\Delta \bar{v}}{\Delta z}\right)^2\right)$.

For the static instability, the buoyancy term is usually negative, and the buoyancy force will suppress the turbulent development; for the neutral stratification, the buoyancy term is usually zero; and for the static stability stratification, the buoyancy is usually positive, which will promote the turbulent development. While the shear term usually has positive value and attribute to the mechanical turbulence. In our study, the averaged buoyancy term is positive and larger than the shear term, leading to the Ri larger than 1, this indicated that the mechanical production rate can not balance the turbulent kinetic energy's consumption by buoyancy. Therefore, from a statistical point of view, the atmospheric turbulence is stable on the BJ, XT and LT stations. Turbulent energy is affected by various factors, except for the buoyancy term and the mechanical product term, there are also the turbulent transport contribution and the dissipation terms. Through analysis of the Ri value is just for a simplify and effective evaluation. Although the averaged result exhibited a more significant effect of buoyancy term than the shear term, there are many different occasions that the Ri is less than 1, and the shear term may play a dominant role.

As we mentioned in line 407-410, the higher buoyancy term in XT may be resulted from the warm advection from the Loess Plateau. Since the warm advection usually develops from southwest to the northeast and results in strong thermal inversion above the NCP plain, the warm advection will has stronger impact at the XT station than the BJ station. Thus, this will lead to a higher buoyancy term contribution in XT.

Comment 2:

Line 381-382: It appears that the profiles were averaged over only two time points (i.e. 8:00 am and 08:00 pm), right? Can the average of only two time points represent the entire day MLH features which are most significant during noon time?

Response 2:

Thank you for your suggestion. Yes, the profiles were averaged over only two time points (i.e. 8:00 am and 08:00 pm). Analysis of these two time points could explain the lower MLH in XT at 8:00 am and 08:00 pm, but could not exactly illustrate the entire day MLH features. Although we can not better explain the day MLH features with these limited data, our study still provide a fundamental knowledge about the reasons for MLH contrast between northern NCP and southern Hebei. We can also make a prediction about these parameters features during noon time: it is known that the MLH development is mainly affected by the solar radiation during daytime and such radiation is almost consistent on the NCP plain, since the XT has weaker turbulent develop condition (i.e., weaker mechanical force and stronger buoyancy inhibition) than the BJ station, the MLH development at the XT station might be weaker than the BJ station. Such limitation in our study is illustrated in the final paragraph of the conclusion section.

Comment 3:

Line 444-447: In addition to the emission discrepancy and different meteorological factors (like MLH), the aerosol-radiation interactions are a potential candidate to explain different PM pollution between the two interested regions. Therefore, it is better to say 60% is the upper bound of contribution due to meteorological factors.

Response 3:

Thank you for your suggestion. Consider your comment, it is certainly reasonable to say 60 % is the upper bound of contribution due to meteorological factors. Therefore, the relevant contents were modified in section 4.3 in our revised manuscript.

Comment 4:

Line 474: a recent ref should also be cited here:

Wang G, et al. (2016) Persistent sulfate formation from London Fog to Chinese haze. Proceedings of the National Academy of Sciences 113(48):13630-13635.

Response 4:

Thank you for your suggestion. The paper that you mentioned has been cited in our revised manuscript.

Comment 5:

Line 409: “enhance” should be “enhanced” or “enhancement of”.

Response 5:

Thank you for your suggestion. We have already modified the relevant content in the revised manuscript.

Mixing layer height on the North China Plain and meteorological

evidence of serious air pollution in southern Hebei

Xiaowan Zhu^{1,2}, Guiqian Tang^{1*}, Jianping Guo³, Bo Hu¹, Tao Song¹, Lili Wang¹, Jinyuan Xin¹, Wenkang Gao¹, Christoph Munkel⁴, Klaus Schäfer⁵, Xin Li^{1,6}, and Yuesi Wang¹

¹State Key Laboratory of Atmospheric Boundary Layer Physics and Atmospheric Chemistry (LAPC), Institute of Atmospheric Physics, Chinese Academy of Sciences, Beijing 100029, China

²University of Chinese Academy of Sciences, Beijing 100049, China

³State Key Laboratory of Severe Weather & Key Laboratory of Atmospheric Chemistry of CMA, Chinese Academy of Meteorological Sciences, Beijing 100081, China

⁴Vaisala GmbH, 22607 Hamburg, Germany

⁵Atmospheric Science College, Chengdu University of Information Technology (CUIT), Chengdu 610225, China

⁶Beijing Municipal Committee of China Association for Promoting Democracy, Beijing 100035, China

Correspondence to: G. Tang (tgq@dq.cern.ac.cn)

Abstract

To investigate the spatiotemporal variability of the mixing layer height (MLH) on the North China Plain (NCP), multi-site and long-term observations of the MLH with ceilometers at three inland stations (Beijing (BJ), Shijiazhuang (SJZ) and Tianjin (TJ)) and one coastal site (Qinhuangdao) were conducted from 16 October 2013 to 15 July 2015. The MLH of the inland stations in the NCP were highest in summer and lowest in winter, while the MLH on the coastal area of Bohai was lowest in summer and highest in spring. As a typical site in southern Hebei, the annual mean of the MLH at SJZ was 464 ± 183 m, which was 15.0 % and 21.9 % lower than that at the BJ (594 ± 183 m) and TJ (546 ± 197 m) stations, respectively. Investigation of the shear term and buoyancy term in the NCP revealed that these two parameters in southern Hebei were 2.8 times lower and 1.5 times higher than that in northern NCP within 0-1200 m in winter, respectively, leading to a 1.9-fold higher frequency of the Gradient Richardson number >1 in southern Hebei compared to the northern NCP. Furthermore, combined with aerosol optical depth and $PM_{2.5}$ observations, we found that the pollutant column concentration contrast (1.2 times) between these two areas was far less than the near-ground $PM_{2.5}$ concentration contrast (1.5 times). Through analysis of the ventilation coefficient in the NCP, the near-ground heavy pollution in southern Hebei mainly resulted from the lower MLH and wind speed. Therefore, due to the importance of unfavorable weather conditions, heavily polluting enterprises should be relocated and strong emission reduction measures are required to improve

43 the air quality in southern Hebei.

44 **1. Introduction**

45 The convective boundary layer is the region where turbulence is fully developed.
46 The height of the interface where turbulence is discontinuous is usually referred to as
47 the mixing layer height (MLH) (Stull, 1988). The mixing layer is regarded as the link
48 between the near-surface and free atmosphere, and the MLH is one of the major
49 factors affecting the atmospheric dissipation ability, which determines both the
50 volume into which ground-emitted pollutants can disperse, as well as the convective
51 time scales within the mixing layer (Seidel et al., 2010). In addition, continuous MLH
52 observations will be of great importance for the improvement of boundary layer
53 parameterization schemes and for the promotion of meteorological model accuracy.

54 Conventionally, the MLH is usually estimated from radiosonde profiles (Seidel et
55 al., 2010). Although meteorological radiosonde observations can provide high-quality
56 data, they are not suitable for continuous fine-resolution MLH retrievals due to their
57 high cost and limited observation intervals (Seibert et al., 2000). As the most
58 advanced method of MLH detection, remote sensing techniques based on the profile
59 measurements from ground-based instruments such as sodar, radar, or lidar that have
60 the unique vertically resolved observational capability are becoming increasingly
61 popular (Beyrich, 1997; Chen et al., 2001; He et al., 2005). Because sound waves can
62 be easily attenuated in the atmosphere, the vertical range of sodar is generally limited
63 to within 1000 m. However, the optical remote sensing techniques can provide higher
64 height ranges (at least several kilometers). The single-lens ceilometers developed by
65 Vaisala have been widely used in a variety of MLH studies (Alexander et al., 2017;
66 Emeis et al., 2004, 2009, 2011; Eresmaa et al., 2006; Munkel et al., 2004, 2007;
67 Muñoz and Undurraga, 2010; Schween et al., 2014; Sokół et al., 2014; Tang et al.,
68 2015, 2016; Wagner et al., 2006, 2015). Compared with other remote sensing
69 instruments, this type of lidar has special features favorable for long-term and
70 multi-station observations (Emeis et al., 2009; Wiegner et al., 2014; Tang et al., 2016),
71 including the low-power system, the eye-safe operation within a near infrared laser
72 band, and the low cost and ease of maintenance during any weather conditions
73 (excluding rainy, strong windy or sandstorm weather conditions) with only regular
74 window cleaning required (Emeis et al., 2004; Tang et al., 2016).

75 The North China Plain (NCP) region is the political, economic and cultural center
76 of China. With the rapid economic development, energy use has increased
77 substantially, resulting in frequent air pollution episodes (Guo et al., 2011; Li et al.,
78 2013; Liu et al., 2016; Tang et al., 2017b; Wang et al., 2014; Wang et al., 2013a; Xu et
79 al., 2016; Zhang et al., 2014). The haze pollution has had an adverse impact on human
80 health (Tang et al., 2017a) and has aroused a great deal of concern (Tang et al., 2009;
81 Ji et al., 2012; Zhang et al., 2015a). To achieve the integrated development of the
82 Jing-Jin-Ji region, readjustment of the regional industrial structure and layout is
83 imperative. To this end, the industrial capacity of heavily polluting enterprises in the
84 areas with unfavorable weather conditions should be reduced, and these heavily
85 polluting enterprises should be removed to improve the air quality. For the remaining
86 enterprises, the industrial air pollutant emissions structure should be changed, and

87 strong emission reduction measures must be implemented. Although the government
88 has carried out some strategies for joint prevention and control, with the less
89 well-understood distributions of regional weather condition on the NCP, how and
90 where to adjust the industrial structures on the NCP are questions in pressing need of
91 answers. As one of the key factors influencing the regional heavy haze pollution
92 (Tang et al., 2012, 2016, 2017b; Quan et al., 2013; Hu et al., 2014; Zhu et al., 2016;
93 Zhang et al., 2016a), the MLH to some extent represents the atmospheric
94 environmental capacity, and the regional distribution and variation of MLH on the
95 NCP can offer a scientific basis for regional industrial distribution readjustment,
96 which will be of great importance for regional haze management.

97 Nevertheless, due to the scarcity of MLH observations on the NCP, reliable and
98 explicit characteristics of MLH on the NCP remain unknown. Tang et al. (2016)
99 utilized the long-term observation data of MLH from ceilometers to analyze the
100 characteristics of MLH variations in Beijing (BJ) and verified the reliability of
101 ceilometers. The results demonstrated that MLH in BJ was high in spring and summer
102 and low in autumn and winter with two transition months in February and September.
103 A multi-station analysis of MLH on the NCP region was conducted in February 2014,
104 and the characteristics of high MLH at coastal stations and low MLH at southwest
105 piedmont stations were reported (Li et al., 2015). Miao et al. (2015) modeled the
106 seasonal variations of MLH on the NCP and discovered that the MLH was high in
107 spring due to the strong mechanical forcing and low in winter as a result of the strong
108 thermodynamic stability in the near-surface layer. The mountain-plain breeze and the
109 sea breeze circulations played an important role in the mixing layer process when the
110 background synoptic patterns were weak in summer and autumn (Tang et al., 2016;
111 Wei et al., 2017).

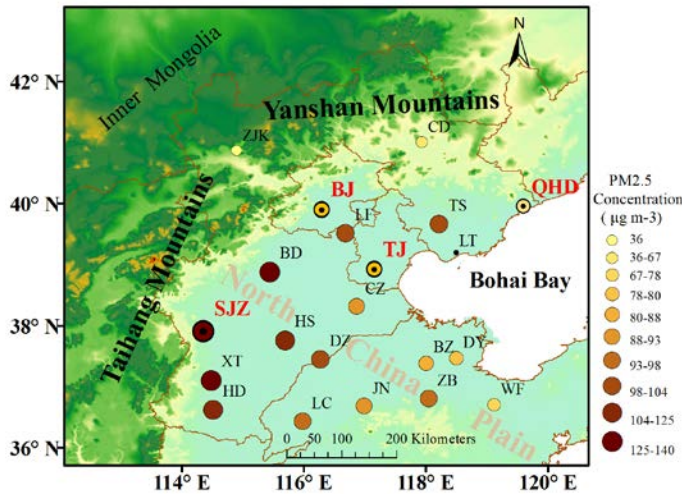
112 To overcome previous studies' deficiencies, our study first conducted a 22-month
113 (from 16 October 2013 to 15 July 2015) observation of MLH with ceilometers on the
114 NCP. The observation stations included three inland stations (BJ, Shijiazhuang (SJZ)
115 and Tianjin (TJ)) and one coastal site (Qinhuangdao (QHD)). First, we will describe
116 the spatial and temporal distribution of MLH on the NCP. Subsequently, reasons for
117 spatial difference of MLH on the NCP will be explained in the discussion section.
118 Finally, the meteorological evidence of serious air pollution in southern Hebei will be
119 studied.

120 **2 Data and methods**

121 **2.1 Sites**

122 To study the MLH characteristics on the NCP, observations with ceilometers were
123 conducted at the BJ, SJZ, TJ and QHD stations from 16 October 2013 to 15 July 2015
124 (Fig. 1 and Table S1). The SJZ, TJ and QHD sites were set around Beijing in the
125 southwest, southeast and east directions, respectively. The BJ station was at the base
126 of the Taihang and Yanshan Mountains on the northern NCP. The MLH observation
127 site was built in the courtyard of the Institute of Atmospheric Physics, Chinese
128 Academy of Sciences (116.32° E, 39.90° N). SJZ was near the Taihang Mountain in
129 southern Hebei; the location was in the Hebei University of Economics (114.26° E,
130 38.03° N). The TJ site was set in the courtyard of the Tianjin Meteorological Bureau,

131 which was located south of the urban area, with a geographic location of 117.20° E,
 132 39.13° N. The QHD station was an eastern coastal site of Bohai Bay, which was set
 133 up in the Environmental Management College of China (119.57° E, 39.95° N), and
 134 the surrounding areas are mostly residential buildings with no high structures. Since
 135 the TJ site was approximately 50 km away from the coast and the QHD station was
 136 only 2 km, the TJ station, by contrast, was supposed to be an inland station.



137
 138 Fig. 1 Locations of the ceilometers observation sites (BJ, SJZ, TJ and QHD) are
 139 marked with red and bold abbreviations; other PM_{2.5} observation sites (ZJK, CD, LF,
 140 TS, CZ, BD, HS, XT, HD, DZ, LC, JN, BZ, DY, ZB and WF) and the sounding
 141 observation sites (BJ, LT and XT) are marked on the map with black abbreviations.
 142 The size and color of the circular mark are representative of the annual mean
 143 near-ground PM_{2.5} concentration; the larger and darker the circle is, the greater the
 144 concentration is.

145 2.2 Measurement of MLH

146 The instrument used to measure the MLH at the four stations was an enhanced
 147 single-lens ceilometer (Vaisala, Finland), which utilized the strobe laser lidar (laser
 148 detection and range measurement) technique (910 nm) to measure the attenuated
 149 backscattering coefficient profiles. As large differences existed in the aerosol
 150 concentrations between the mixing layer and the free atmosphere, the MLH can be
 151 determined from the vertical attenuated backscattering coefficient (β) gradient,
 152 whereby a strong, sudden change in the negative gradient ($-d\beta/dx$) can indicate the
 153 MLH. In the present study, the Vaisala software product BL-VIEW was utilized to
 154 calculate the MLH by determining the location of the maximum $|-d\beta/dx|$ in the
 155 attenuated backscattering coefficient. To strengthen the echo signals and reduce the
 156 detection noise, spatial and temporal averaging should be conducted before the
 157 gradient method is used to calculate the MLH. The BL-VIEW software was utilized
 158 with temporal smoothing of 1200 s and vertical distance smoothing of 240 m. The
 159 instrument installed at the BJ station was a CL31 ceilometer and the CL51

160 ceilometers were used at the SJZ, TJ and QHD stations. Some of the properties of
 161 these two instruments are listed in Table 1, and basic technical descriptions can be
 162 found in Munkel et al. (2007) and Tang et al. (2015).

163 To ensure the consistency of the MLH measurements with the two different
 164 ceilometer versions, before we set up the ceilometer observation network in the NCP,
 165 we made a comparison of the MLHs observed by CL31 and CL51 at BJ from October
 166 1 to October 8, 2013 (Fig. S1). The MLH observed by CL31 was highly relevant to
 167 those observed by the CL51 ceilometers, with correlation coefficients (R) of 0.86-0.92.
 168 Therefore, the impact of version discrepancy on the MLH measurement can be
 169 neglected.

170 Since the ceilometers can reflect rainy conditions and the precipitation will
 171 influence the MLH retrieval, the precipitation data were excluded. In addition, a
 172 previous study has compared MLH measurements retrieved from ceilometers and
 173 sounding data (Tang et al., 2016). The results revealed that the ceilometers
 174 underestimate the MLH under neutral conditions caused by strong winds and
 175 overestimate the MLH when sand storms occur. Therefore, data points for these three
 176 special weather conditions were eliminated manually. The criterion to exclude these
 177 data points is as follows: (a) precipitation, i.e., a cloud base lower than 4000 m and
 178 the attenuated backscattering coefficient of at least $2 \times 10^{-6} \text{ m}^{-1} \text{ sr}^{-1}$ within 0 m and the
 179 cloud base, (b) sandstorm, i.e., the ratio of $\text{PM}_{2.5}$ to PM_{10} suddenly decreased to 30 %
 180 or lower and the PM_{10} concentration was higher than $500 \mu\text{g m}^{-3}$, and (c) strong winds,
 181 i.e., a sudden change in temperature and wind speed (WS) when cold fronts passed by
 182 (Muñoz and Undurraga, 2010; Tang et al., 2016; Van der Kamp and McKendry,
 183 2010).

184 Table 1 Instrument properties of CL31 and CL51

Parameter	CL31	CL51
Detection range (km)	7.57	153.0
Wavelength (nm)	910	910
Report period (s)	2-120	6-120
<u>Measurement interval</u>		
<u>(s)Report accuracy-</u>	<u>25</u>	<u>640</u>
<u>(m)</u>		
<u>Measurement</u>		
<u>resolution (m)Peak-</u>	<u>10340</u>	<u>10340</u>
<u>power (W)</u>		

带格式表格

185 2.3 Other data

186 The hourly data of near-ground relative humidity (RH) and temperature (T) in the
 187 NCP region were obtained from the China Meteorological Administration
 188 (<http://www.weather.com.cn/weather/101010100.shtml/>). To study the reason for the
 189 MLH difference between the northern NCP and southern Hebei, meteorological
 190 sounding data were included in this paper. The data were provided by the upgraded
 191 radiosonde network of China, where the GTS1 digital electronic radiosonde was
 192 required to be operationally launched twice per day at 08:00 LT and 20:00 LT by the
 193 China Meteorological Administration (Guo et al., 2016). Considering the deficiency

194 of sounding data at the SJZ and QHD stations, data from the Xingtai (XT) and
 195 Laoting (LT) stations were used instead after a consistency test with the reanalysis
 196 data (Fig. S2). The reanalysis data at these four sites were downloaded from the
 197 website of European Centre for Medium-Range Weather Forecasts
 198 (<http://apps.ecmwf.int/datasets/data/interim-full-mnth/levtype=pl/>).

199 The near-ground PM_{2.5} and PM₁₀ concentrations at the 20 observation sites from
 200 December 2013 to November 2014 were provided by the Ministry of Environmental
 201 Protection with a time resolution of 1 h (<http://www.zhb.gov.cn/>). Details for the
 202 near-ground PM_{2.5} and PM₁₀ observation sites are shown in Table S1 and Fig. 1.

203 The aerosol optical depth (AOD) data within the NCP region were retrieved with
 204 the dark target algorithm from the Moderate Resolution Imaging Spectra-radiometer
 205 aerosol products on board the National Aeronautics and Space Administration Earth
 206 Observing System Terra satellite from December 2013 to November 2014 (Zhang et
 207 al., 2016b) (<https://ladsweb.nascom.nasa.gov/search/index.html/>), then the AOD data
 208 was interpolated into 0.1°×0.1° to produce the regional distribution in the NCP.

209 **2.4 Atmospheric stability criterion**

210 The Gradient Richardson number (*Ri*) is usually used to estimate the atmospheric
 211 turbulent stability within the mixing layer and is defined as follows (Eq. 1):

$$212 \quad Ri = \frac{\frac{g\Delta\bar{\theta}}{\bar{\theta}\Delta z}}{\left(\frac{\Delta\bar{u}}{\Delta z}\right)^2 + \left(\frac{\Delta\bar{v}}{\Delta z}\right)^2} \quad (1)$$

213 Where Δz is the height increment over which a specific calculation of *Ri* is being
 214 made; g is the acceleration of gravity; $\bar{\theta}$ is the mean virtual potential temperature
 215 within that height increment; and $\Delta\bar{u}$ and $\Delta\bar{v}$ are the mean wind speeds in zonal and
 216 meridional directions within the height increment.

217 Using *Ri* to diagnose turbulence is a classical approach and has been covered in
 218 many textbooks on boundary-layer turbulence (Stull, 1988; Garratt, 1994). It can be
 219 interpreted as the ratio of the buoyancy term $\left(\frac{g\Delta\bar{\theta}}{\bar{\theta}\Delta z}\right)$ to the shear term $\left(\left(\frac{\Delta\bar{u}}{\Delta z}\right)^2 + \left(\frac{\Delta\bar{v}}{\Delta z}\right)^2\right)$
 220 in the turbulent kinetic equation. When the $Ri > 1$, the turbulence was
 221 suppressed and the mixing layer development will be restrained (Stull, 1988). In our
 222 study, the frequency of $Ri > 1$ was used to represent the atmospheric stability in the
 223 NCP. The larger the frequency is, the more stable turbulent stratification is.

224 **3. Results**

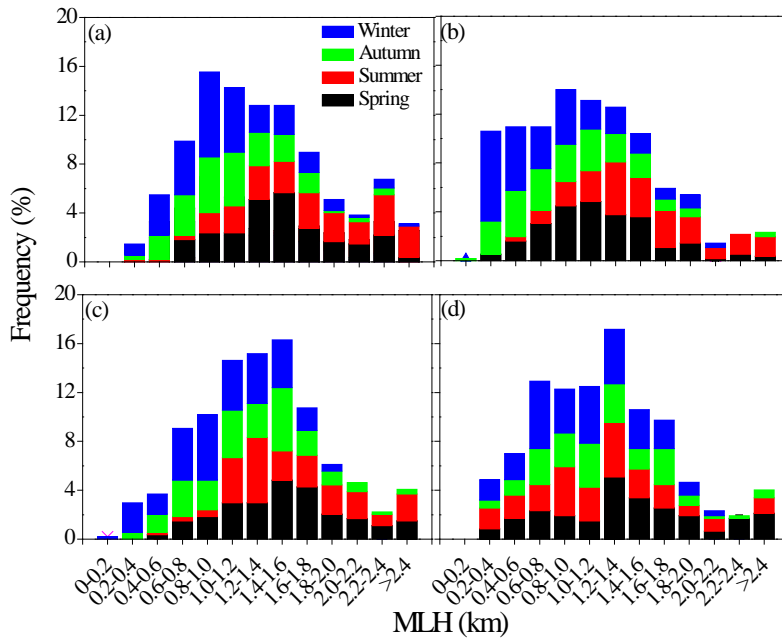
225 **3.1 Frequency distribution of MLH**

226 Since October 2013, continuous operation of the ceilometers observation network
 227 in the NCP has provided 22 months of MLH data. For the purpose of analyzing the
 228 MLH temporal and spatial variation, the hourly averages of MLH for a whole year
 229 (from December 2013 to November 2014) at the BJ, SJZ, TJ and QHD stations were
 230 chosen in the following sections. Hourly means of MLH under rainy, sandstorm and
 231 windy conditions were removed, resulting in data availability of 81, 89, 83 and 77 %
 232 at the BJ, SJZ, TJ and QHD stations, respectively. In this study, March, April and May
 233 are defined as spring; June, July and August are defined as summer; September,

234 October and November are defined as autumn; and December, January and February
 235 are defined as winter.

236 To study the regional distribution characteristic of MLH on the NCP, we analyzed
 237 the frequency of the daily maximum MLH distribution in Fig. 2. The daily maximum
 238 MLH at the BJ, SJZ and TJ stations could reach 2400 m. The large daily maximum
 239 values mostly existed in spring and summer, while the low values always appeared in
 240 autumn and winter and were as low as 200 m. The daily maximum MLH values at the
 241 BJ, SJZ and TJ stations were mainly distributed between 600 and 1800 m, 400 and
 242 1600 m and 800 and 1800 m, accounting for 74.2, 72.0 and 67.0 % of the total
 243 samples, respectively. Notably, the daily maximum MLH in SJZ was lower than at the
 244 MLHs at the BJ and TJ stations in spring, autumn and winter. Values below 600 m at
 245 the SJZ station occurred primarily in autumn and winter. The most frequent daily
 246 maximum MLH existed in the range of 1000-1200 m, which was 200-600 m lower
 247 than that at the TJ station. This demonstrated a weaker atmospheric diffusion
 248 capability at the SJZ station in spring, autumn and winter than the northern NCP
 249 stations.

250 The frequency distribution of the daily maximum MLH at the coastal site showed
 251 different features. The daily maximum MLH in QHD was mainly distributed between
 252 800 and 1800 m with a relatively small seasonal fluctuation (Fig. 2d). Values lower
 253 than 600 m were mainly distributed in summer, which was probably influenced by the
 254 frequent occurrence of a thermal internal boundary layer (TIBL) in summer. Reasons
 255 for this are illustrated in section 4.1.



256
 257 Fig. 2 Frequency distribution of the daily maximum MLH at the (a) BJ, (b) SJZ, (c)
 258 TJ and (d) QHD stations from December 2013 to November 2014.

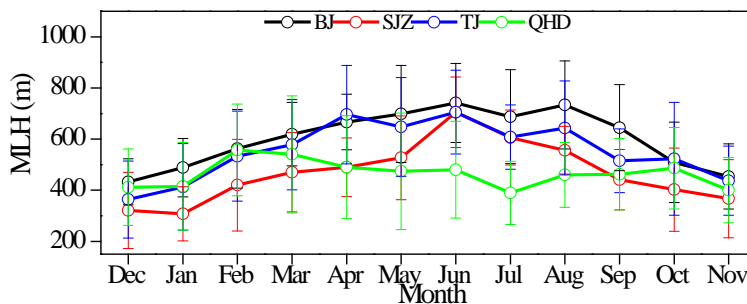
259 **3.2 Spatiotemporal variation of MLH**

260 **3.2.1 Seasonal variation**

261 Monthly variations of MLH at the BJ, SJZ, TJ and QHD stations are shown in Fig.
262 3. The monthly means of the regional MLH ranged between 300 and 750 m. The
263 maximum and minimum MLH existed in June 2014 at the BJ station and in January
264 2014 at the SJZ station, with values of 741 and 308 m, respectively. Most of the
265 monthly averages were between 400 and 700 m, which accounted for 81.3 % of the
266 total samples.

267 The MLH at the BJ, SJZ and TJ stations showed obvious seasonal variations with
268 high values in spring and summer and low values in autumn and winter. Seasonal
269 means of MLH at the three stations followed the same order:
270 summer>spring>autumn>winter, with maximum values of 722 ± 169 , 623 ± 161 and
271 655 ± 165 m in summer, respectively, and minimum values of 493 ± 131 , 347 ± 153 and
272 436 ± 178 m in winter, respectively (Table S2). Obvious annual changes of the MLH
273 with large values in spring and summer and low values in autumn and winter at the BJ,
274 SJZ and TJ stations implied that MLH is influenced by seasonal changes of solar
275 radiation (Stull, 1988).

276 Nevertheless, the seasonal variation of MLH at the coastal site of Bohai was
277 different from that at the inland stations. The MLH in QHD exhibited a decreasing
278 trend from spring to summer and an increasing trend from autumn to winter, with the
279 maximum seasonal mean of 498 ± 217 m in spring and the minimum seasonal mean of
280 447 ± 153 m in summer. Moreover, the MLH in spring and summer at QHD was much
281 lower than those at other stations. Similar to our analysis of frequency distributions of
282 daily maximum MLH in section 3.1, the lower MLH at QHD in spring and summer
283 mainly resulted from the frequent occurrence of the TIBL. A detailed explanation of
284 the TIBL impact was included in section 4.1. The effect of TIBL on the coastal
285 boundary layer was consistent with previous studies (Zhang et al., 2013; Tu et al.,
286 2012), which demonstrated that ceilometers can properly retrieve the coastal MLH as
287 well.



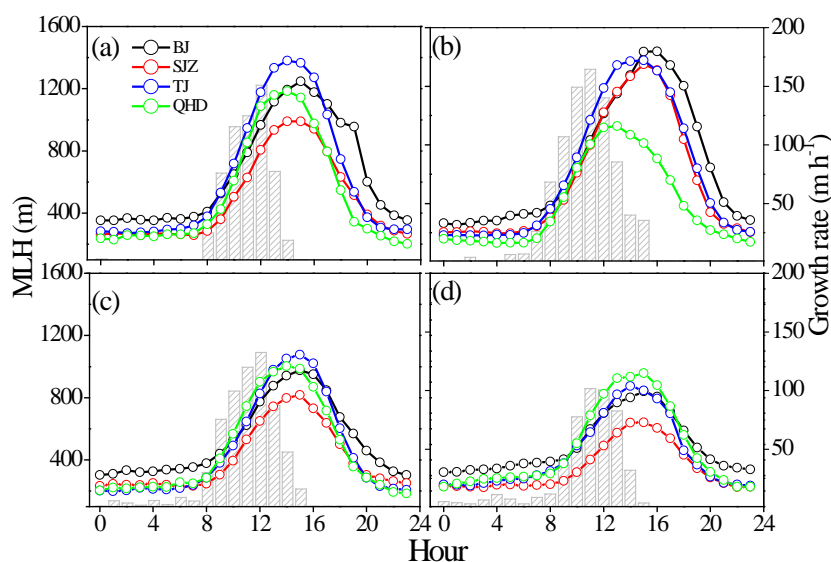
288
289 Fig. 3 Monthly variations of MLH at the BJ, SJZ, TJ and QHD stations from
290 December 2013 to November 2014.

291 **3.2.2 Diurnal variations**

292 Seasonal variations of diurnal MLH change patterns were investigated to reveal the
293 24 h evolution characteristics of the MLH on the NCP. As shown in Fig. 4, diurnal
294 variations of MLH in different seasons all had single peak patterns. With sunrise and

295 increased solar radiation, MLH at the four stations started to develop and peaked in
 296 the early afternoon. After sunset, turbulence in the MLH decayed quickly, and the
 297 mixing layer underwent a transition to the nocturnal stable layer (less than 400 m).
 298 The annual averaged diurnal ranges of MLH at the BJ, SJZ, TJ and QHD stations
 299 were 782, 699, 914 and 790 m, respectively. The annual averaged diurnal range of
 300 MLH in SJZ was approximately 100-200 m smaller than those at the other stations,
 301 which was associated with its shallow daytime MLHs in spring, autumn and winter
 302 (Figs. 4a, 4c and 4d). This also indicated the worse pollutant diffusion ability in SJZ.

303 Growth rates averaged over the four stations during each season were plotted with
 304 gray columns in Fig. 4. It was obvious that the growth rates of the MLH varied by
 305 season. The MLH developed the earliest in summer (at approximately 7:00 LT) and
 306 reached the highest growth rates (164.5 m h^{-1}) at approximately 11:00 LT, and the
 307 time when MLH started to develop was found to be 1 hour later (at approximately
 308 8:00 LT) in spring and autumn than in summer. Furthermore, the MLH developed the
 309 latest (at approximately 9:00 LT) and slowest in winter, with the maximum growth
 310 rate (101.8 m h^{-1}) occurring at approximately 11:00 LT.



311
 312 Fig. 4 Diurnal variations of MLH at the BJ, SJZ, TJ and QHD stations in (a) spring, (b)
 313 summer, (c) autumn and (d) winter seasons are indicated by lines and scatters. The
 314 growth rates averaged over the four sites are drawn with gray columns for each season
 315 to represent the MLH growth velocity, and only positive values are shown in the
 316 figure.

317 Annual averages of MLH at the BJ, SJZ, TJ and QHD stations were also calculated,
 318 and the values were 594 ± 183 , 464 ± 183 , 546 ± 197 and 465 ± 175 m, respectively. The
 319 MLH at SJZ was approximately 21.9, 15.0 and 0.2 % lower than at the BJ, TJ and
 320 QHD stations, respectively. Therefore, according to the analysis above in sections 3.1
 321 and 3.2, an obvious phenomenon can be observed in the MLH distribution on the
 322 NCP: the MLH in southern Hebei was lower than in the northern NCP in spring,

323 autumn and winter but was almost equal to the northern areas in summer.

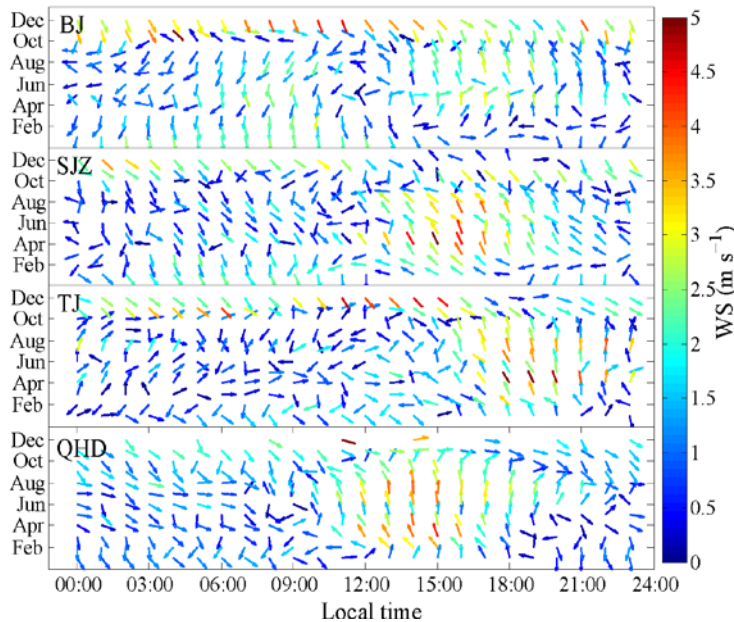
324 **4. Discussion**

325 Through preliminary study of the spatiotemporal variation of MLH on the NCP
326 region, we found something interesting: (a) the MLH at the coastal site was lower
327 than the inland sites in summer; (b) the MLH in southern Hebei was lower than the
328 northern NCP in spring, autumn and winter, but was almost consistent between these
329 two areas in summer. Reasons for these two phenomena will be illustrated in the
330 following sections (4.1 and 4.2). Finally, we will investigate the meteorological
331 evidence for serious haze pollution in southern Hebei in section 4.3.

332 **4.1 The TIBL impact in coastal site**

333 From the studies in sections 3.1 and 3.2, we found that the maximum MLH at the
334 QHD station was larger and arrived earlier than the BJ, SJZ and TJ stations in summer
335 (Fig. 4b). However, this characteristic was not evident in other seasons (Figs. 4a, 4c
336 and 4d). The sea-land breeze was a local circulation that occurs when there is no
337 large-scale synoptic system passes. In our study, we first excluded days with
338 large-scale synoptic systems. Then, according to the coastline orientation, if the
339 southeast wind at the TJ station and south and southwest winds at the QHD station
340 occurred at approximately 11:00 LT, and the northwest wind started to blow at
341 approximately 20:00 LT, then this type of circulation was supposed to be a sea-land
342 circulation. The prevailing southeast wind at the TJ station and the south and
343 southwest wind at the QHD station were regarded as sea breezes (Fig. 5).

344 The sea breeze usually brings a cold and stable air mass from the sea to the coastal
345 region. When the top of the local mixing layer was higher than the top of the air mass,
346 a TIBL will develop within the mixing layer under the influence of the abrupt change
347 of aerodynamic roughness and temperature between the land and sea surfaces. Then,
348 the local mixing layer will be replaced by the TIBL. In the presence of warm air on
349 land, the cold sea air advects downwind and is warmed, leading to a weak temperature
350 difference between the air and the ground. In consequence, the TIBL warms less
351 rapidly due to the decreased heat flux at the ground, and the rise rate is reduced. In
352 addition, since the TIBL deepens with distance downwind and usually can not extend
353 all the way to the top of the intruding marine air, the remaining cool marine air above
354 the TIBL will hinder vertical development of the TIBL (Stull, 1988; Sicard et al.,
355 2006; Puygrenier et al., 2005; Tomasi et al., 2011). With distance inland, the top of
356 the intruding marine air will enhance and exceed the local MLH; if so, the TIBL will
357 not form, and the TIBL impact will be impaired with distance inland (Stull, 1988).
358 Accompanied by the weak synoptic system and the frequent occurrence of sea breezes
359 in summer, the TIBL formed easily and the MLH peak time and value at the QHD
360 station were earlier and lower than other stations (Figs. 3 and 4). For the TJ station,
361 with a distance of approximately 50 km out to sea, the TIBL will not extend so far.
362 Therefore, although the TJ station can be affected by the sea breeze, the local MLH
363 cannot be influenced by the TIBL.

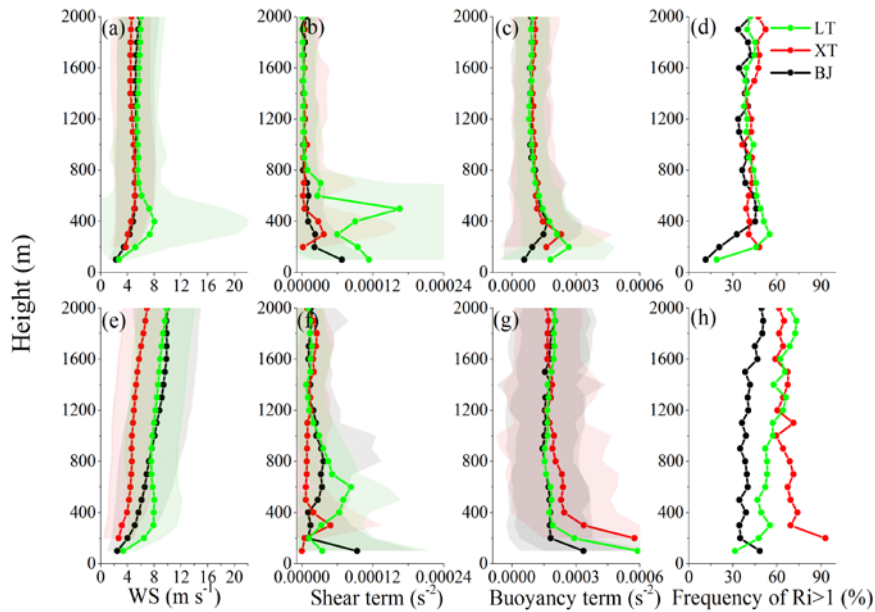


364

365 Fig. 5 Monthly diurnal wind vectors at the BJ, SJZ, TJ and QHD stations from
 366 December 2013 to November 2014.

367 **4.2 Reasons for low MLH in southern Hebei**

368 Turbulent stability was mainly responsible for the MLH development, and the
 369 generation of turbulent energy was highly correlated with the heat flux (mainly
 370 sensible heat fluxes) produced by radiation and the momentum flux caused by wind
 371 shear (Stull, 1988). As presented in section 2.4, the Ri could describe the turbulent
 372 stability not only from the perspective of thermal forces but also from the perspective
 373 of mechanical forces; it was calculated in this section with meteorological sounding
 374 profiles to study the reason for MLH differences between southern Hebei and the
 375 northern NCP, and the frequency values of $Ri > 1$ were given in this study. With larger
 376 frequency comes more stable stratification. Considering the geographic locations (Fig.
 377 1), the lack of sounding data at the SJZ station was replaced by sounding data from
 378 the XT station; meanwhile, sounding data from the LT station was used instead of the
 379 data from QHD. Each of the four parameter profiles (WS, shear term, buoyancy term,
 380 and the frequency of $Ri > 1$) at the BJ, XT and LT stations are depicted in Fig. 6. The
 381 profiles were averaged over 8:00 LT and 20:00 LT and vertically smoothed using a
 382 100-m running average to reduce unexpected fluctuations for viewing purposes only.



383

384

385

386

387

388

389

390

391

392

393

394

395

396

397

398

399

400

401

402

403

404

405

406

407

408

409

Fig. 6 Vertical profiles of (a, e) horizontal WS, (b, f) shear term, (c, g) buoyancy term and (d, h) frequency of $Ri>1$ at the BJ, XT and LT stations in summer (upper panel) and winter (lower panel).

Using the winter and summer as examples, when we analyzed the seasonal means of shear term and the buoyancy term between the XT and the BJ stations, some distinct features were observed. As shown in Figs. 6f and 6g, the shear term and the buoyancy term in XT was 2.8 times lower and 1.5 times higher than that in BJ within 0-1200 m in winter, respectively. The largest discrepancies of the wind shear term and buoyancy term between southern Hebei and the northern NCP could reach $2.84 \times 10^{-5} \text{ s}^{-2}$ at the altitude of 800 m and $3.93 \times 10^{-4} \text{ s}^{-2}$ at 200 m, respectively. As a result, the frequency of $Ri>1$ in XT was approximately 1.9 times larger than that in BJ within 0-1200 m, leading to a much more stable stratification in southern Hebei (Fig. 6h). The shear term, buoyancy term and the frequency of $Ri>1$ in spring and autumn displayed similar characteristics to those in winter, and the averaged frequency of $Ri>1$ in southern Hebei was approximately 1.5 and 1.3 times larger than those in northern NCP in spring and autumn, respectively (Fig. S3). While in summer, the shear term, buoyancy term and the frequency of $Ri>1$ were almost the same between southern Hebei and the northern NCP (Figs. 6b, 6c and 6d).

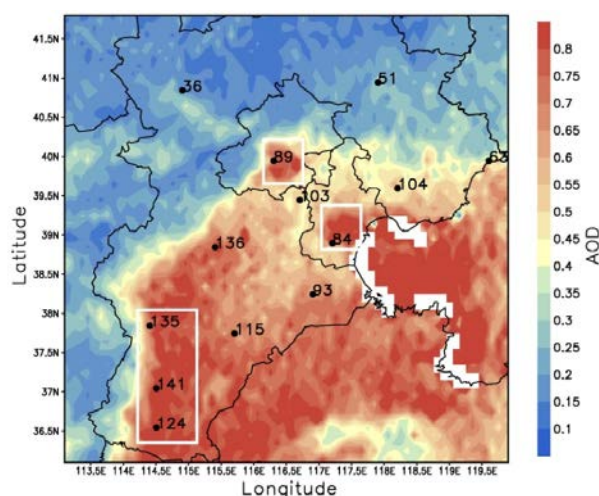
As a result, the lower MLH in southern Hebei was due to a more stable atmospheric turbulent structure than the northern NCP in spring, autumn and winter. This probably resulted from the frequent effect of cold air on the northern NCP, and such cold air was usually too weak to reach southern Hebei (Su et al., 2004). Then the cold front resulting from the cold air system will enhance the wind shear over the northern NCP. In addition, a previous study has revealed that the warm advection from the Loess Plateau usually developed from south_{west} to north_{east}, and the higher buoyancy term (Fig. 6g) and lower MLH in southern Hebei will be partially related to the enhanced

410 thermal inversion at the altitude of 1500 m (Hu et al., 2014; Zhu et al., 2016). In
411 summer, due to the northward lift and westward intrusion of the subtropical high on
412 the NCP, the diminishing existence of the weak cold air on the northern NCP
413 accompanied with the regional scale strong solar radiation and strong turbulent
414 activities will lead to a small turbulent stability contrast between southern Hebei and
415 the northern NCP.

416 In addition, other researchers proposed that absorbing aerosols above the MLH can
417 be another factor affecting the MLH (Peng et al., 2016; Wang et al., 2013; Li et al.,
418 2016). Absorbing aerosols gives rise to an increasing temperature aloft but a
419 decreasing temperature at the surface, which will enhance the strength of capping
420 inversion and inhibit the convective ability. In contrast, absorbing aerosols within the
421 mixing layer could reduce the capping inversion intensity despite the reduction in the
422 surface buoyancy flux and raise the MLH (Yu et al., 2002). Considering the higher
423 concentrations of surface PM_{2.5} in southern Hebei, absorbing aerosols could have
424 some impacts on MLH development. However, the comprehensive influences from
425 the feedback of absorbing aerosols above and below the MLH are hard to explain
426 without sufficient knowledge of vertical variations in absorbing aerosols at the four
427 stations. Additionally, the mixed state and morphology of absorbing aerosols
428 dominant the absorption effects (Jacobson, 2001; Bond et al., 2013). Therefore,
429 without sufficient observation data, it is difficult to discuss the possible influences of
430 air pollution feedback on MLH development in this study. Elaborate experiments of
431 vertical profiles and the morphology of absorbing aerosols are needed in future
432 studies.

433 **4.3 Meteorological evidence of serious air pollution in southern Hebei**

434 When we analyzed the near-ground PM_{2.5} and PM₁₀ concentration distributions on
435 the NCP from December 2013 to November 2014, a unique phenomenon was found
436 and shown in Fig. 1 and Fig. S4. The annual means of near-ground PM_{2.5}
437 concentration in southern Hebei (SJZ, XT and HD) was 133.3 $\mu\text{g m}^{-3}$ (225.3 $\mu\text{g m}^{-3}$
438 for the PM₁₀ concentrations), while in the northern areas (BJ and TJ), it was 86.5 $\mu\text{g m}^{-3}$
439 (126.0 $\mu\text{g m}^{-3}$ for the PM₁₀ concentrations), and the difference in the near-ground
440 PM_{2.5} concentration between the two areas can be as high as 1.5-fold (1.8-fold for the
441 PM₁₀ concentrations). Since AOD represents the aerosol column concentration, it is a
442 much better indicator for the emissions difference than the PM_{2.5}. Additionally, the
443 averaged annual AOD in southern Hebei was only 1.2 times of that in the northern
444 NCP (Fig. 7). If the difference in AOD represents the emission discrepancy, the
445 remaining differences of PM_{2.5} may be induced by the meteorology. In other words,
446 meteorological conditions may play an important role in heavier haze formation in
447 southern Hebei and the meteorological condition contrast between these two areas
448 may contributed at most approximately 60% (considering the aerosol-radiation
449 interactions) to the PM_{2.5} concentration discrepancy.



450

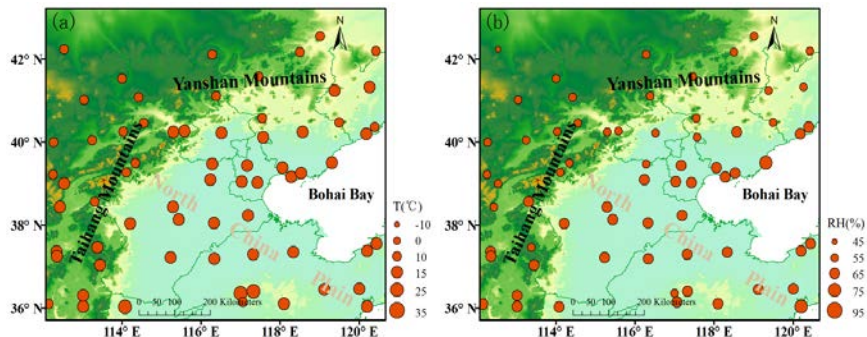
451 Fig. 7 Distribution of the annual mean values of AOD from December 2013 to
 452 November 2014 in the NCP. The $PM_{2.5}$ concentrations of the 13 observation sites
 453 were also marked beside each station. The major sites in the northern NCP (BJ and TJ)
 454 and southern Hebei (SJZ, XT and HD) are enclosed by white rectangles.

455 Previous studies revealed that the most significant meteorological factors for
 456 regional heavy haze formation in the NCP were RH and MLH (Tang et al., 2016; Zhu
 457 et al., 2016). In addition, the T influences the particles' physicochemical reaction rate
 458 and the ventilation coefficients (V_c) can be used as an index to evaluate the total
 459 diffusion ability of the atmosphere; thus, the RH, T and V_c were compared and
 460 analyzed among the four stations (BJ, SJZ, TJ and QHD) in the next section. The
 461 regional particle growth and the atmospheric dissipation ability will be discussed
 462 separately, each from a meteorological point of view.

463 4.3.1 Meteorological factors for particle growth

464 Distributions of annual means of T and RH are shown in Fig. 8, and the
 465 distributions of seasonal means of T and RH were added in Figs. S5 and S6. The T
 466 value in southern Hebei was similar to that on the northern NCP but was higher than
 467 that at the coastal site (Figs. 8a and S5). This indicated an almost consistent
 468 temperature condition for an atmospheric physicochemical reaction (Garratt et al.,
 469 1994; Zhang et al., 2010). However, differences existed in RH between southern
 470 Hebei and the northern NCP. The RH in the SJZ station was always higher than that in
 471 the BJ and TJ stations but was slightly lower than that at the coastal sites (Figs. 8b and
 472 S6). The annual averages of RH at the BJ, SJZ, TJ and QHD sites were 51.2, 65.7,
 473 57.0 and 68.6 %, respectively, and the RH at SJZ was 22.1 and 13.2 % higher than
 474 that at the BJ and TJ sites, respectively (Table S3). Since RH is a key factor for haze
 475 development, higher RH is beneficial to fine particle growth through hygroscopic
 476 growth processes and heterogeneous reactions (Zhao et al., 2013; Fu et al., 2014; Liu
 477 et al., 2011; Hu et al., 2006; [Wang et al., 2016](#); Zhang et al., 2015; Seinfeld et al.,
 478 1998). Thus, a higher RH provided a favorable meteorological condition for haze
 479 development, which could be partially responsible for heavier pollution in southern

480 Hebei.



481
482 Fig. 8 Distribution of annual means of (a) T and (b) RH in the NCP region from
483 December 2013 to November 2014.

484 4.3.2 Meteorological factors for particle dissipation

485 As MLH and WS can represent the atmospheric dissipation capability in the
486 vertical and horizontal directions, respectively, in addition to the MLH, we analyzed
487 the WS variations on the NCP. Similar to our analysis in section 4.2, as SJZ and QHD
488 had no sounding data and due to the close geographic proximity among SJZ and XT
489 as well as LT and QHD, sounding data from the XT and LT stations were used instead
490 of the data at SJZ and QHD, respectively. The WS profiles were averaged every 100
491 m at each station and are depicted in Figs. 6 and S3. Except for summer, the WS in
492 southern Hebei was far less than that on the northern NCP in spring, autumn and
493 winter (Figs. 6e, S3a and S3e) but was nearly consistent in summer (Fig. 6a). This
494 finding indicated a weaker horizontal diffusion capability in southern Hebei than that
495 on the northern NCP.

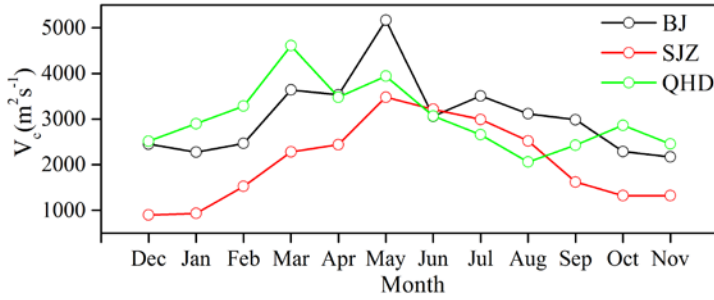
496 The V_c is an important factor in pollutant dissipation and air quality studies; it
497 accounts for the vertical dispersion and advection of pollutants. With a larger V_c ,
498 strong dissipation ability follows. The V_c is defined as the product of MLH and wind
499 transport (U_T) as shown in Eq. (2).

$$500 V_c = \text{MLH} \times U_T \quad (2)$$

501 When we utilized the wind profiles in Figs. 6 and S3 with equal spacing in the vertical
502 direction, U_T could be regarded as the mean wind transport, i.e., $U_T = \frac{1}{n} \sum_{i=1}^n U_i$ where

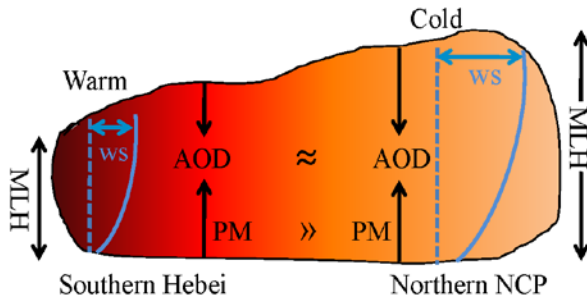
503 U_i is the WS observed at each level and n is the number of levels within the mixing
504 layer (Nair et al., 2007). Since the WS was a climatic parameter, the WS profiles at
505 08:00 LT and 20:00 LT were used to approximate V_c approximately. Considering the
506 monthly averaged MLH at the BJ, SJZ and QHD stations, the monthly V_c were
507 depicted in Fig. 9. V_c at southern Hebei was always lower than that in the northern
508 NCP during the whole study period. The seasonal means of V_c at the BJ, SJZ and
509 QHD stations in spring, summer, autumn and winter were 4112.0, 2733.3 and 4008.5;
510 3227.5, 2908.8 and 2593.7; 2481.4, 1421.9 and 2581.7; and 2397.2, 1117.7 and
511 2900.0 $\text{m}^2 \text{s}^{-1}$, respectively. It was clear that the SJZ station usually had the lowest V_c ,
512 and the annual averaged V_c at SJZ was almost 1.5 and 1.5 times smaller than the BJ
513 and QHD stations, respectively (Table S3). As a result, the particle dissipation

514 capability in southern Hebei was much weaker than that in the northern NCP and
 515 coastal areas.
 516



517
 518 Fig. 9 Seasonal variations of V_c at the BJ, SJZ and QHD stations from December
 519 2013 to November 2014. The V_c is defined as the product of MLH and wind transport
 520 (Nair et al., 2007) (Eq. (2)). With a larger V_c , strong dissipation ability follows.

521 Therefore, with lower MLH, lower WS and higher RH occur in southern Hebei
 522 compared to the northern NCP, the near-ground $PM_{2.5}$ showed a large contrast
 523 between these two areas. However, the AOD had little difference between southern
 524 Hebei and the northern NCP. Apart from the emission contrast, the meteorological
 525 condition contrast between these two areas heavily contributed to the heavy haze in
 526 southern Hebei and the industrial structure is in need of readjustment for the NCP (Fig.
 527 10).



528
 529 Fig.10 The schematic diagram of the meteorological causes for heavy haze in
 530 southern Hebei.

531 **5. Conclusions**

532 To gain new insight into the spatiotemporal variation of the regional MLH, the
 533 present study conducted a simultaneous observation with ceilometers at three inland
 534 stations (BJ, SJZ, and TJ) and one coastal site (QHD) to obtain high spatial and
 535 temporal resolution MLH data. The experiment period lasted for 22-months from
 536 October 16, 2013, to July 15, 2015, and a whole year of data (from December 2013 to
 537 November 2014) were utilized for further study. Conclusions were drawn as follows.

538 The ceilometers can not only retrieve the inland MLH but also retrieve the coastal
 539 MLH properly. The MLHs in the inland areas of the NCP were high in spring and

540 summer and low in autumn and winter. While under the impact of TIBL, the coastal
541 MLH had an opposite variation trend of inland sites and the lowest MLH in QHD
542 occurred in summer. The TIBL impaired the local MLH development at the coastal
543 site and caused the mixing layer to peak early in summer; this effect weakened with
544 distance inland.

545 The MLH in southern Hebei was lower than that on the northern NCP, especially in
546 spring, autumn and winter. This mainly resulted from the more stable turbulent
547 structure (weak shear term, higher buoyancy term and larger frequency of $Ri > 1$) than
548 the northern NCP, and the stable stratification in southern Hebei was partially related
549 to the Siberian High and warm advection from the Loess Plateau. In summer, the
550 atmospheric stability was almost consistent between southern Hebei and the northern
551 NCP, and the MLHs between these two areas were nearly identical.

552 The lower MLH and WS in southern Hebei restricted the atmospheric
553 environmental capability and the pollutant dissipation ability, respectively.
554 Accompanied by higher RH values (stronger pollutant growth ability), the adverse
555 weather conditions will cause severe haze to occur easily in southern Hebei, and the
556 industrial layout in the NCP is in need of restructuring. Heavily polluting enterprises
557 should be relocated to locations with better weather conditions (e.g., some northern
558 areas and coastal areas), and strong emission reduction measures should be
559 implemented in the remaining industrial enterprises to improve air quality.

560 Overall, the present study is the first to conduct a long-term observation of the
561 MLH with high spatial and temporal resolution on a regional scale. The observation
562 results will be of great importance for model parameterization scheme promotion and
563 provide basic information for the distribution of weather conditions in the NCP region.
564 The deficiency of this study is that we did not account for the transport effect on
565 $PM_{2.5}$ concentrations. Because pollutants are usually transported from south to north
566 in the NCP region during haze episodes (Zhu et al., 2016; Tang et al., 2015), pollutant
567 transport has a greater impact on the northern areas and has less influence on the
568 results of this analysis. The absence of sounding data at noon is another shortcoming,
569 and the daytime observations will be implemented in future experiments.
570 Nevertheless, with the data only at 8:00 LT and 20:00 LT, we still provide a
571 fundamental knowledge about the reasons for MLH contrast between northern NCP
572 and southern Hebei, and our study can provide reasonable and scientific suggestions
573 for industrial layout and air pollution emission reduction measures for the NCP
574 region, ~~which~~ This will be of great importance for achieving the integrated
575 development goals.

576 **Acknowledgments**

577 This work was supported by the National Key R&D Program of China
578 (2017YFC0210000), the National Natural Science Foundation of China (41705113),
579 the Beijing Municipal Science and Technology Project (ZL171100000617002) and
580 the National Earth System Science Data Sharing Infrastructure, National Science &
581 Technology Infrastructure of China.

582
583

584 **References**

585

586

Beyrich, F.: Mixing height estimation from SODAR data – a critical discussion, Atmos. Environ., 31, 3941–3953, 1997.

587

Bond, T. C., Doherty, S. J., Fahey, D. W., et al.: Bounding the role of black carbon in the climate system: a scientific assessment, J. Geophys. Res., 118, 1-173, doi:10.1002/jgrd.50171, 2013.

589

590

Chen, W. B., Kuze, H., Uchiyama, A., Suzuki, Y., and Takeuchi, N.: One-year observation of urban mixed layer characteristics at Tsukuba, Japan using a micro pulse lidar, Atmos. Environ., 35, 4273–4280, doi:10.1016/S1352-2310(01)00181-9, 2001.

593

594

Emeis, S., Münkkel, C., Vogt, S., Müller, W. J., and Schäfer, K.: Atmospheric boundary-layer structure from simultaneous SODAR, RASS, and ceilometer measurements, Atmos. Environ., 38(2), 273-286, doi:10.1016/j.atmosenv.2003.09.054, 2004.

597

598

Emeis, S., Schäfer, K., and Münkkel, C.: Observation of the structure of the urban boundary layer with different ceilometers and validation by RASS data, Meteorologische Zeitschrift, 18(2), 149-154, doi:10.1127/0941-2948/2009/0365, 2009.

599

600

Emeis, S., Schäfer, K., Münkkel, C., Friedl, R., and Suppan, P.: Evaluation of the Interpretation of Ceilometer Data with RASS and Radiosonde Data, Bound.-Lay. Meteorol., 143(1), 25-35, doi:10.1007/s10546-011-9604-6, 2011.

604

605

Eresmaa, N., Karppinen, A., Joffre, S. M., Nen, J. R. S., and Talvitie, H.: Mixing height determination by ceilometer, Atmos. Chem. Phys., 6, 1485–1493, doi:10.5194/acp-6-1485-2006, 2006.

606

607

Fu, G. Q., Xu, W. Y., Yang, R. F., Li, J. B., and Zhao, C. S.: The distribution and trends of fog and haze in the North China Plain over the past 30 years, Atmos. Chem. Phys., 14 (21), 11949-11958, 2014.

609

610

Garratt, J.: The atmospheric boundary layer. Cambridge University Press, U.K., 316, 1994.

612

613

Geiß, A., Wiegner, M., Bonn, B., Schäfer, K., Forkel, R., Schneidmesser, E. V., Münkkel, C., Chan, K. L., and Nothard, R. Alexander, G., M. Wiegner, B. Bonn, K. Schäfer, R. Forkel, E. Schneidmesser, C. Münkkel, K. Chan, and R. Nothard: Mixing layer height as an indicator for urban air quality? Atmos. Meas. Tech., 10, 2969-2988, doi.org/10.5194/amt-10-2969-2017, 2017.

614

615

Guo, J. P., Miao, Y., Zhang, Y., Liu, H., Li, Z., Zhang, W., He, J., Lou, M., Yan, Y., Bian, L., and Zhai, P.: The climatology of planetary boundary layer height in China derived from radiosonde and reanalysis data, Atmos. Chem. Phys., 16(20), 13309-13319, doi:10.5194/acp-16-13309-2016, 2016.

620

621

Guo, J., Zhang, X., Wu, Y., Che, H., Laba, and Li, X.: Spatio-temporal variation trends of satellite-based aerosol optical depth in China during 1980-2008, Atmos. Environ., 45(37), 6802-6811, doi: 10.1016/j.atmosenv.2011.03.068, 2011.

624

625

He, Q. S., and Mao, J. T.: He, Q. and Mao, J.: Observation of urban mixed layer at

626

627

带格式的: 缩进: 左侧: 0 厘米, 悬挂缩进: 2.5 字符, 首行缩进: -2.5 字符

带格式的: EndNote Bibliography, 两端对齐, 定义网格后自动调整右缩进, 调整中文与西文文字的间距, 调整中文与数字的间距

带格式的: 缩进: 左侧: 0 厘米, 悬挂缩进: 2.5 字符, 首行缩进: -2.5 字符

带格式的

628 [Beijing using a micro pulse lidar, Acta Meteorol. Sin., 63, 374–384, 2005.](#)

629 [Hu, M., Liu, S., Wu, Z. J., Zhang, J., Zhao, Y. L., Wehner, B., and Wiedensohler, A.: Effects of high temperature, high relative humidity and rain process on particle size distributions in the summer of Beijing, Environ. Sci., 27\(11\), 2006.](#)

630

631

632 [Hu, X. M., Ma, Z. Q., Lin, W. L., Zhang, H. L., Hu, J. L., Wang, Y., Xu, X. B., Fuentes, J. D., and Xue, M.: Impact of the Loess Plateau on the atmospheric boundary layer structure and air quality in the North China Plain?: A case study, Sci. Total Environ., 499, 228–237, doi:10.1016/j.scitotenv.2014.08.053, 2014.](#)

633

634

635

636 [Jacobson, M. Z.: Strong radiative heating due to the mixing state of black carbon in atmospheric aerosols, Nature, 409,695-697, 2001.](#)

637

638 [Ji, D. S., Wang, Y. S., Wang, L. L., Chen, L. F., Hu, B., Tang, G. Q., Xin, J. Y., Song, T., Wen, T. X., Sun, Y., Pan, Y. P., and Liu, Z. R.: Analysis of heavy pollution episodes in selected cities of northern China, Atmos. Environ., 50\(2012\), 338-348, 2012.](#)

639

640

641

642 [Jing, T. U., Zhang, S. P., Cheng, X. K., Yang, W. Y., and Yang, Y. Q.: Temporal and Spatial Variation of Atmospheric Boundary Layer Height\(ABLH\) over the Yellow East China Sea, J. Ocean U. China, 42\(4\):7-18, 2012.](#)

643

644

645 [Kamp, D. V. D., and Mckendry, I.: Diurnal and Seasonal Trends in Convective Mixed-Layer Heights Estimated from Two Years of Continuous Ceilometer Observations in Vancouver, BC, Bound.-Lay. Meteorol., 137\(3\), 459-475, doi:10.1007/s10546-010-9535-7, 2010.](#)

646

647

648

649 [Li, M., Tang, G. Q., Huang, X. J., Liu, Z. R., An, J. L., and Wang, Y. S.: Relationship between atmospheric MLH and winter haze pollution in the Jing-Jin-Ji region, Environ. Sci., 2015,\(06\):1935-1943, 2015.](#)

650

651

652 [Li, P., Xin, J. Y., Bai, X. P., Wang, Y. S., Wang, S. G., Liu, S. X., and Feng, X. X.: Observational studies and a statistical early warning of surface ozone pollution in Tangshan, the largest heavy industry city of North China, Inter. J. Env. Res. Pub. Heal., 10\(3\), 1048-1061, doi:10.3390/ijerph10031048, 2013.](#)

653

654

655

656 [Li, Z. Q., Lau, W. K., Ramanathan, V. et al.: Aeosol and monsoon climate interactions over Asia, Rev. Geophys., 54, 886-929, doi:10.1002/2015RG000500, 2016.](#)

657

658 [Liu, Z. R., Hu, B., Zhang, J., Yu, Y., and Wang, Y. S.: Characteristics of aerosol size distributions and chemical compositions during wintertime pollution episodes in Beijing, Atmos. Res., 168, 1-12, doi:10.1016/j.atmosres.2015.08.013, 2016.](#)

659

660

661 [Liu, Z. R., Sun, Y., Li, L., and Wang, Y. S.: Particle mass concentrations and size distribution during and after the Beijing Olympic Games, Environ. Sci., 32\(4\), doi:10.13227/j.hjlx.2011.04.015, 2011.](#)

662

663

664 [Miao, Y. C., Hu, X. M., Liu, S. H., Qian, T. T., Xue, M., Zheng, Y. J., and Wang, S.: Seasonal variation of local atmospheric circulations and boundary layer structure in the Beijing-Tianjin-Hebei region and implications for air quality, J. Adv. Model. Earth. Sy., 7\(4\), 1602-1626, doi:10.1002/2015ms000522, 2015.](#)

665

666

667

668 [Münkel, C., and Räsänen, J.: New optical concept for commercial lidar ceilometers scanning the boundary layer, P.SPIE, 5571, 364-374, 2004.](#)

669

670 [Münkel, C., Eresmaa, N., Räsänen, J., and Karppinen, A.: Retrieval of mixing height and dust concentration with lidar ceilometer, Bound.-Lay. Meteorol., 124\(1\),](#)

671

带格式的: EndNote Bibliography, 两端对齐, 缩进: 左侧: 0 厘米, 悬挂缩进: 2.5 字符, 首行缩进: -2.5 字符, 定义网格后自动调整右缩进, 调整中文与西文文字的间距, 调整中文与数字的间距

带格式的

带格式的: 缩进: 左侧: 0 厘米, 悬挂缩进: 2.5 字符, 首行缩进: -2.5 字符

带格式的: EndNote Bibliography, 两端对齐, 定义网格后自动调整右缩进, 调整中文与西文文字的间距, 调整中文与数字的间距

带格式的: 缩进: 左侧: 0 厘米, 悬挂缩进: 2.5 字符, 首行缩进: -2.5 字符

带格式的: EndNote Bibliography, 两端对齐, 缩进: 左侧: 0 厘米, 悬挂缩进: 2.5 字符, 首行缩进: -2.5 字符, 定义网格后自动调整右缩进, 调整中文与西文文字的间距, 调整中文与数字的间距

带格式的

带格式的: 缩进: 左侧: 0 厘米, 悬挂缩进: 2.5 字符, 首行缩进: -2.5 字符

672 [117-128, doi:10.1007/s10546-006-9103-3, 2007.](#)

673 [Muñoz, R. C., and Undurraga, A. A.: Daytime Mixing layer over the Santiago Basin:](#)

674 [Description of Two Years of Observations with a Lidar Ceilometer, J. Appl.](#)

675 [Meteorol. Clim., 49\(8\), 1728-1741, doi:10.1175/2010jamc2347.1, 2010.](#)

676 [Nair, V. S., Moorthy, K. K., and Alappattu, D. P. et al.: Wintertime aerosol](#)

677 [characteristics over the Indo-Gangetic Plain \(IGP\): Impacts of local boundary](#)

678 [layer processes and long-rang transport, J. Geo. Res.: 2006JD008099,](#)

679 [doi:10.1029/2006JD008099, 2007.](#)

680 [Peng, J. F., Hu, M., Guo, S., Du, Z. F., Zheng, J., Shang, D. J., Misti, L. Z., Zeng, L.](#)

681 [M., Shao, M., Wu, Y. S., Zheng, J., Wang, Y., Glen, C. R., Collins, D. R., and](#)

682 [Molina, M. J.: Markedly enhanced absorption and direct radiative forcing of](#)

683 [black carbon under polluted urban environments, P. Natl. Acad. Sci. Usa.,](#)

684 [113\(4266-4271\), doi:10.1073/pnas.1602310113, 2016.](#)

685 [Puygrenier, V., F. Lohou, B. Campistron, F. Saïd, G. Pigeon, B. Bénech, and D. Serça:](#)

686 [Investigation on the fine structure of sea-breeze during ESCOMPTE](#)

687 [experiment, Atmos. Res., 74\(1-4\), 329-353,](#)

688 [doi:http://dx.doi.org/10.1016/j.atmosres.2004.06.011, 2005.](#)

689 [Quan, J. N., Gao, Y., Zhang, Q., Tie, X. X., Cao, J. J., Han, S. Q., Meng, J. W., Chen,](#)

690 [P. F., and Zhao, D. L.: Evolution of planetary boundary layer under different](#)

691 [weather conditions, and its impact on aerosol concentrations, Particuology, 11,](#)

692 [34-40, doi:10.1016/j.partic.2012.04.005, 2013.](#)

693 [Schween, J. H., Hirsikko, A., Löhnert, U., and Crewell, S.: Mixing-layer height](#)

694 [retrieval with ceilometer and Doppler lidar: from case studies to long-term](#)

695 [assessment, Atmos. Meas. Tech., 7\(11\), 3685-3704,](#)

696 [doi:10.5194/amt-7-3685-2014, 2014.](#)

697 [Seibert, P., Beyrich, F., Gryng, S. E., Joffre, S., Rasmussen, A., and Tercier, P.:](#)

698 [Review and intercomparison of operational methods for the determination of](#)

699 [the mixing height, Atmos. Environ., 34\(7\), 1001-1027,](#)

700 [doi:http://dx.doi.org/10.1016/S1352-2310\(99\)00349-0, 2000.](#)

701 [Seidel, D. J., Ao, C. O., and Li, K.: Estimating climatological planetary boundary](#)

702 [layer heights from radiosonde observations: Comparison of methods and](#)

703 [uncertainty analysis, J. Geophys. Res., 115, D16113,](#)

704 [doi:10.1029/2009JD013680, 2010.](#)

705 [Seinfeld, J., and Pandis, S.: Atmospheric Chemistry and Physics: From Air Pollution](#)

706 [to Climate Change, New York: John Wiley and Sons, 1998.](#)

707 [Sicard, M., Pérez, C., Rocadenbosch, F., Baldasano, J. M., and García-Vizcaino, D.:](#)

708 [Mixed-Layer Depth Determination in the Barcelona Coastal Area From Regular](#)

709 [Lidar Measurements: Methods, Results and Limitations. Boundary-Layer](#)

710 [Meteorology 119, 135-157, 2006.](#)

711 [Sokół, P., Stachlewska, I. S., Ungureanu, I., and Stefan, S.: Evaluation of the](#)

712 [boundary layer morning transition using the CL-31 ceilometer signals, Acta](#)

713 [Geophys., 62\(2\), doi:10.2478/s11600-013-0158-5, 2014.](#)

714 [Stull, R.: An Introduction to Boundary Layer Meteorology, Kluwer Academic](#)

715 [Publishers, Dordrecht, 1988.](#)

716 [Su, F. Q., Yang, M. Z., Zhong, J. H., and Zhang, Z. G.: The effects of synoptic type on](#)
717 [regional atmospheric contamination in North China, Res. Of Environ. Sci.,](#)
718 [17\(3\), doi:10.13198/j.res.2004.03.18.sufq.006, 2004.](#)

719 [Tang, G. Q., Li, X., Wang, Y. S., and Xin, J. Y.: Surface ozone trend details and](#)
720 [interpretations in Beijing, 2001–2006, Atmos. Chem. Phys., 9, 8813-8823,](#)
721 [doi:10.5194/acp-9-8813-2009, 2009.](#)

722 [Tang, G. Q., Wang, Y. S., Li, X., Ji, D. S., Hsu, S., and Gao, X.: Spatial-temporal](#)
723 [variations in surface ozone in Northern China as observed during 2009–2010](#)
724 [and possible implications for future air quality control strategies, Atmos. Chem.](#)
725 [Phys., 12, 2757-2776, doi:10.5194/acp-12-2757-2012, 2012.](#)

726 [Tang, G. Q., Zhang, J. Q., Zhu, X. W., Song, T., Munkel, C., Hu, B., Schäfer, K., Liu,](#)
727 [Z. R., Zhang, J. K., Wang, L. L., Xin, J. Y., Suppan, P., and Wang, Y. S.: Mixing](#)
728 [layer height and its implications for air pollution over Beijing, China, Atmos.](#)
729 [Chem. Phys., 16\(4\), 2459-2475, doi:10.5194/acp-16-2459-2016, 2016.](#)

730 [Tang, G. Q., Zhao, P. S., Wang, Y. H., Gao, W. K., Cheng, M. T., Xin, J. Y., Li, X., and](#)
731 [Wang, Y. S.: Mortality and air pollution in Beijing: the long-term relationship,](#)
732 [Atmos. Environ., 150, 238-243, doi: 10.1016/j.atmosenv.2016.11.045, 2017a.](#)

733 [Tang, G. Q., Zhu, X. W., Hu, B., Xin, J. Y., Wang, L. L., Munkel, C., Mao, G., and](#)
734 [Wang, Y. S.: Impact of emission controls on air quality in Beijing during APEC](#)
735 [2014: lidar ceilometer observations, Atmos. Chem. Phys., 15\(21\), 12667-12680,](#)
736 [doi:10.5194/acp-15-12667-2015, 2015.](#)

737 [Tang, G. Q., Zhu, X. W., Xin, J. Y., Hu, B., Song, T., Sun, Y., Zhang, J. Q., Wang, L.](#)
738 [L., Cheng, M. T., Chao, N., Kong, L. B., Li, X., and Wang, Y. S.: Modelling](#)
739 [study of boundary-layer ozone over northern China - Part I: Ozone budget in](#)
740 [summer. Atmos. Res., 187, 128-137, 2017b.](#)

741 [Tomasi, F. D., Miglietta, M. M., and Perrone, M. R.: a Case Study, Bound.-Lay.](#)
742 [Meteorol., 139:521-541, doi: 10.1007/s10546-011-9592-6, 2011.](#)

743 [Wagner, M., Emeis, S., Freudenthaler, V., Heese, B., Junkermann, W., Munkel, C.,](#)
744 [Schäfer, K., Seefeldner, M., and Vogt, S.: Mixing layer height over Munich,](#)
745 [Germany: Variability and comparisons of different methodologies, J. Geophys.](#)
746 [Res., 111, D13201, doi:10.1029/2005JD006593, 2006.](#)

747 [Wagner, P. and Schäfer, K.: Influence of mixing layer height on air pollutant](#)
748 [concentrations in an urban street canyon, Urban Climate,](#)
749 [http://dx.doi.org/10.1016/j.uclim.2015.11.001, 2015.](#)

750 [Wang, G. H., Zhang, R. Y., and Gómesz, M. E. et al.: Persistent sulfate formation](#)
751 [from London Fog to Chinese haze, P. Natl. Acad. Sci., 113\(48\):13630-13635,](#)
752 [doi: 10.1073/pnas.1616540113, 2016.](#)

753 [Wang, L. L., Zhang, N., Liu, Z. R., Sun, Y., Ji, D. S., and Wang, Y. S.: The Influence](#)
754 [of Climate Factors, Meteorological Conditions, and Boundary-Layer Structure](#)
755 [on Severe Haze Pollution in the Beijing-Tianjin-Hebei Region during January](#)
756 [2013, Adv. Meteorol., 2014, 1-14, doi:10.1155/2014/685971, 2014.](#)

757 [Wang, Y. S., Yao, L., Wang, L. L., Liu, Z. R., Ji, D. S., Tang, G. Q., Zhang, J. K., Sun,](#)
758 [Y., Hu, B., and Xin, J. Y.: Mechanism for the formation of the January 2013](#)
759 [heavy haze pollution episode over central and eastern China, Sci. China Earth](#)

带格式的: 字体: (默认) Times
New Roman, 小四

760 [Sci.](#), 57(1), 14-25, doi:10.1007/s11430-013-4773-4, 2013a.

761 [Wang, Y., Khalizov, A., Levy, M., and Zhang, R. Y.: New Directions: Light absorbing](#)

762 [aersols and their atmospheric impacts, Atmos. Environ.](#), 81, 713-715, doi:

763 [10.1016/j.atmosenv.2013.09.034, 2013b.](#)

764 [Wei, J., Tang, G. Q., Zhu, X. W., Wang, L. L., Liu, Z. R., Cheng, M. T., Munkel, C.,](#)

765 [Li, X., and Wang, Y. S.: Thermal internal boundary layer and its effects on air](#)

766 [pollutants during summer in a coastal city in North China, Journal of](#)

767 [Environmental Sciences](#), 1001-0742, doi:10.1016/j.jes.2017.11.006, 2017.

768 [Wiegner, M., Madonna, F., Biniotoglou, I., Forkel, R., Gasteiger, J., Geiß, A.,](#)

769 [Pappalardo, G., Schäfer, K., and Thomas, W.: What is the benefit of ceilometers](#)

770 [for aerosol remote sensing? An answer from ERALINET, Atmos. Meas. Tech.](#),

771 [7, 1979-1997, doi: 10.5194/amt-7-1979-2014, 2014.](#)

772 [Xu, R. G., Tang, G. Q., Wang, Y. S., and Tie, X. X: Analysis of a long-term](#)

773 [measurement of air pollutants \(2007-2011\) in North China Plain \(NCP\): Impact](#)

774 [of emission reduction during the Beijing Olympic Games, Chemosphere](#), 159,

775 [647-658, doi:10.1016/j.chemosphere.2016.06.025, 2016.](#)

776 [Yu, H., Liu, S. C., and Dickinson, R. E.: Radiative effects of aerosols on the evolution](#)

777 [of the atmospheric boundary layer, J. Geo. Res.: Atmos.](#), 107, D12(4142),

778 [doi:10.1029/2001JD000754, 2002.](#)

779 [Zhang, H., Wang, Y., Hu, J., Ying, Q., and Hu, X. M.: Relationships between](#)

780 [meteorological parameters and criteria air pollutants in three megacities in](#)

781 [China, Environ. Res.](#), 140, 242-254, doi:10.1016/j.envres.2015.04.004, 2015a.

782 [Zhang, J. K., Sun, Y., Liu, Z. R., Ji, D. S., Hu, B., Liu, Q., and Wang, Y. S.:](#)

783 [Characterization of submicron aerosols during a month of serious pollution in](#)

784 [Beijing, 2013, Atmos. Chem. Phys.](#), 14(6), 2887-2903,

785 [doi:10.5194/acp-14-2887-2014, 2014.](#)

786 [Zhang, Q., Xin, J. Y., Yin, Y., Wang, L. L., and Wang, Y. S.: The Variation and Trends](#)

787 [of MODIS C5 & C6 Products' Errors in the Recent Decade over the](#)

788 [Background and Urban Areas of North China, Remote Sensing](#), 8(9), 754,

789 [doi:10.3390/rs8090754, 2016b.](#)

790 [Zhang, R. Y., Wang, G. H., Guo, S., Zamora, M. L., Ying, Q., Lin, Y., Wang, W. G.,](#)

791 [Hu, M., and Wang, Y.: Formation of Urban Fine Particulate Matter, Chem. Rev.](#),

792 [115, 3803-3855, doi: 10.1021/acs.chemrev.5b00067, 2015b.](#)

793 [Zhang, R. Y.: Getting to the Critical Nucleus of Aerosol Formation, Science](#),

794 [328\(5984\), 1366-1367, doi: 10.1126/science.1189732, 2010.](#)

795 [Zhang, W. C., Guo, J. P., Miao, Y. C., Liu, H., Zhang, Y., Li, Z. Q., and Zhai, P. M.:](#)

796 [Planetary boundary layer height from CALIOP compared to radiosonde over](#)

797 [China, Atmos. Chem. Phys.](#), 16, 9951-9963, doi: 10.5194/acp-16-9951-2016,

798 [2016a.](#)

799 [Zhang, Z. Z., Cai, X. H., Song, Y., Kang, L., Huang, X., and Li, Q. Y.: Temporal and](#)

800 [spatial variation of atmospheric boundary layer height over Hainan Island and](#)

801 [its adjacent sea areas, Acta. Sci. Nat. Univ. Pekin.](#), 49:83-90, doi:

802 [10.13209/j.0479-8023.2013.105, 2013.](#)

803 [Zhao, X. J., Zhao, P. S., Xu, J., Meng, W., Pu, W. W., Dong, F., He, D., and Shi, Q. F.:](#)

带格式的: EndNote Bibliography,
两端对齐, 定义网格后自动调整
右缩进, 调整中文与西文文字的间
距, 调整中文与数字的间距

带格式的

带格式的: 英语(美国)

带格式的: 缩进: 左侧: 0 厘米,
悬挂缩进: 2.5 字符, 首行缩进:
-2.5 字符

804 [Analysis of a winter regional haze event and its formation mechanism in the](#)
805 [North China Plain, Atmos. Chem. Phys., 13 \(11\), 5685-5696, 2013.](#)
806 [Zhu, X. W., Tang, G. Q., Hu, B., Wang, L. L., Xin, J. Y., Zhang, J. K., Liu, Z. R.,](#)
807 [Münkel, C., and Wang, Y. S.: Regional pollution and its formation mechanism](#)
808 [over North China Plain: A case study with ceilometer observations and model](#)
809 [simulations, J. Geo. Res.: Atmos., 2016JD025730, doi:10.1002/2016JD025730,](#)
810 [2016.](#)
811 [Alexander, G., M. Wiegner, B. Bonn, K. Schäfer, R. Forkel, E. Schneidemesser, C.](#)
812 [Münkel, K. Chan, and R. Nothard: Mixing layer height as an indicator for urban](#)
813 [air quality? Atmos. Meas. Tech., 10, 2969-2988,](#)
814 [doi.org/10.5194/amt-10-2969-2017, 2017.](#)
815 [Beyrich, F.: Mixing height estimation from SODAR data—a critical discussion,](#)
816 [Atmos. Environ., 31, 3941-3953, 1997.](#)
817 [Bond, T., S. Doherty, D. Fahery et al.: Bounding the role of black carbon in the](#)
818 [climate system: a scientific assessment, J. Geophys. Res., 118, 1-173,](#)
819 [doi:10.1002/jgrd.50171, 2013.](#)
820 [Chen, W., H. Kuze, A. Uchiyama, Y. Suzuki, and N. Takeuchi: One year observation](#)
821 [of urban mixed layer characteristics at Tsukuba, Japan using a micro-pulse lidar,](#)
822 [Atmos. Environ., 35, 4273-4280, doi:10.1016/S1352-2310\(01\)00181-9, 2001.](#)
823 [Emeis, S., C. Münkel, S. Vogt, W. Müller, and K. Schäfer: Atmospheric](#)
824 [boundary layer structure from simultaneous SODAR, RASS, and ceilometer](#)
825 [measurements, Atmos. Environ., 38\(2\), 273-286,](#)
826 [doi:10.1016/j.atmosenv.2003.09.054, 2004.](#)
827 [Emeis, S., K. Schäfer, and C. Münkel: Observation of the structure of the urban](#)
828 [boundary layer with different ceilometers and validation by RASS data,](#)
829 [Meteorologische Zeitschrift, 18\(2\), 149-154, doi:10.1127/0941-2948/2009/0365,](#)
830 [2009.](#)
831 [Emeis, S., K. Schäfer, C. Münkel, R. Friedl, and P. Suppan: Evaluation of the](#)
832 [Interpretation of Ceilometer Data with RASS and Radiosonde Data, Bound. Lay.](#)
833 [Meteorol., 143\(1\), 25-35, doi:10.1007/s10546-011-9604-6, 2011.](#)
834 [Eresmaa, N., A. Karppinen, S. Joffe, J. Räsänen, and H. Talvitie: Mixing height](#)
835 [determination by ceilometer, Atmos. Chem. Phys., 6, 1485-1493, doi:](#)
836 [10.5194/acp-6-1485-2006, 2006.](#)
837 [Fu, G., W. Xu, R. Yang, J. Li, and C. Zhao: The distribution and trends of fog and](#)
838 [haze in the North China Plain over the past 30 years, Atmos. Chem. Phys., 14](#)
839 [\(21\), 11949-11958, 2014.](#)
840 [Garratt, J.: The atmospheric boundary layer. Cambridge University Press, U.K., 316,](#)
841 [1994.](#)
842 [Guo, J., Y. Miao, Y. Zhang, H. Liu, Z. Li, W. Zhang, J. He, M. Lou, Y. Yan, L. Bian,](#)
843 [and P. Zhai: The climatology of planetary boundary layer height in China derived](#)
844 [from radiosonde and reanalysis data, Atmos. Chem. Phys., 16\(20\), 13309-13319,](#)
845 [doi:10.5194/acp-16-13309-2016, 2016.](#)
846 [Guo, J., X. Zhang, Y. Wu, H. Che, Laba, and X. Li: Spatio-temporal variation trends](#)
847 [of satellite based aerosol optical depth in China during 1980-2008, Atmos.](#)

848 Environ., 45(37), 6802–6811, doi: 10.1016/j.atmosenv.2011.03.068, 2011.

849 He, Q. and Mao, J.: Observation of urban mixed layer at Beijing using a micro-pulse
850 lidar, *Acta Meteorol. Sin.*, 63, 374–384, 2005.

851 Hu, M., S. Liu, Z. Wu, J. Zhang, Y. Zhao, W. Birgit, and W. Alfred: Effects of high
852 temperature, high relative humidity and rain process on particle size distributions
853 in the summer of Beijing, *Environ. Sci.*, 27(11), 2006.

854 Hu, X., Z. Ma, W. Lin, H. Zhang, J. Hu, Y. Wang, X. Xu, J. Fuentes, and M. Xue:
855 Impact of the Loess Plateau on the atmospheric boundary layer structure and air
856 quality in the North China Plain?: A case study, *Sci. Total Environ.*, 499,
857 228–237, doi:10.1016/j.scitotenv.2014.08.053, 2014.

858 Jacobson, M.: Strong radiative heating due to the mixing state of black carbon in
859 atmospheric aerosols, *Nature*, 409, 695–697, 2001.

860 Ji, D., Y. Wang, L. Wang, L. Chen, B. Hu, G. Tang, J. Xin, T. Song, T. Wen, Y. Sun, Y.
861 Pan, Z. Liu: Analysis of heavy pollution episodes in selected cities of northern
862 China, *Atmos. Environ.*, 50(2012), 338–348, 2012.

863 Li, M., G. Tang, J. Huang, Z. Liu, J. An, and Y. Wang: Relationship between
864 atmospheric MLH and winter haze pollution in the Jing Jin Ji region, *Environ.
865 Sci.*, 2015,(06):1935–1943, 2015.

866 Li, P., J. Xin, X. Bai, Y. Wang, S. Wang, S. Liu, and X. Feng: Observational studies
867 and a statistical early warning of surface ozone pollution in Tangshan, the largest
868 heavy industry city of North China, *Inter. J. Env. Res. Pub. Heal.*, 10(3),
869 1048–1061, doi:10.3390/ijerph10031048, 2013.

870 Li, Z., W. Lau, and V. Ramanathan et al.: Aerosol and monsoon climate interactions
871 over Asia, *Rev. Geophys.*, 54, 886–929, doi:10.1002/2015RG000500, 2016.

872 Liu, Z., Y. Sun, L. Li and Y. Wang: Particle mass concentrations and size distribution
873 during and after the Beijing Olympic Games, *Environ. Sci.*, 32(4),
874 doi:10.13227/j.hjlx.2011.04.015, 2011.

875 Liu, Z., B. Hu, J. Zhang, Y. Yu, and Y. Wang: Characteristics of aerosol size
876 distributions and chemical compositions during wintertime pollution episodes in
877 Beijing, *Atmos. Res.*, 168, 1–12, doi:10.1016/j.atmosres.2015.08.013, 2016.

878 Miao, Y., X. Hu, S. Liu, T. Qian, M. Xue, Y. Zheng, and S. Wang: Seasonal variation
879 of local atmospheric circulations and boundary layer structure in the
880 Beijing Tianjin Hebei region and implications for air quality, *J. Adv. Model.
881 Earth. Sy.*, 7(4), 1602–1626, doi:10.1002/2015ms000522, 2015.

882 Münkler, C., and J. Räsänen: New optical concept for commercial lidar ceilometers
883 scanning the boundary layer, *P.SPIE*, 5571, 364–374, 2004.

884 Münkler, C., N. Eresmaa, J. Räsänen, and A. Karppinen: Retrieval of mixing height
885 and dust concentration with lidar ceilometer, *Bound. Lay. Meteorol.*, 124(1),
886 117–128, doi:10.1007/s10546-006-9103-3, 2007.

887 Muñoz, R., and A. Undurraga: Daytime Mixing layer over the Santiago Basin:
888 Description of Two Years of Observations with a Lidar Ceilometer, *J. Appl.
889 Meteorol. Clim.*, 49(8), 1728–1741, doi:10.1175/2010jame2347.1, 2010.

890 Peng, J., M. Hu, S. Guo, Z. Du, J. Zheng, D. Shang, M. Zamora, L. Zeng, M. Shao, Y.
891 Wu, J. Zheng, Y. Wang, C. Glen, D. Collins, M. Molina, and R. Zhang: Markedly

892 enhanced absorption and direct radiative forcing of black carbon under polluted
893 urban environments, *P. Natl. Acad. Sci. Usa.*, 113(4266-4271),
894 doi:10.1073/pnas.1602310113, 2016.

895 Puygrenier, V., F. Lohou, B. Campistron, F. Saïd, G. Pigeon, B. Bénéch, and D. Sereq:
896 Investigation on the fine structure of sea breeze during ESCOMPTE experiment,
897 *Atmos. Res.*, 74(1-4), 329-353,
898 doi:http://dx.doi.org/10.1016/j.atmosres.2004.06.011, 2005.

899 Quan, J., Y. Gao, Q. Zhang, X. Tie, J. Cao, S. Han, J. Meng, P. Chen, and D. Zhao:
900 Evolution of planetary boundary layer under different weather conditions, and its
901 impact on aerosol concentrations, *Particuology*, 11, 34-40,
902 doi:10.1016/j.partic.2012.04.005, 2013.

903 Schween, J., A. Hirsikko, U. Löhnert, and S. Crewell: Mixing layer height retrieval
904 with ceilometer and Doppler lidar: from case studies to long-term assessment,
905 *Atmos. Meas. Tech.*, 7(11), 3685-3704, doi:10.5194/amt-7-3685-2014, 2014.

906 Seibert, P., F. Beyrich, S. Gryning, S. Joffre, A. Rasmussen, and P. Tercier: Review
907 and intercomparison of operational methods for the determination of the mixing
908 height, *Atmos. Environ.*, 34(7), 1001-1027,
909 doi:http://dx.doi.org/10.1016/S1352-2310(99)00349-0, 2000.

910 Seidel, D., C. Ao, and K. Li: Estimating climatological planetary boundary layer
911 heights from radiosonde observations: Comparison of methods and uncertainty
912 analysis, *J. Geophys. Res.*, 115, D16113, doi:10.1029/2009JD013680, 2010.

913 Seinfeld, J. and S. Pandis: *Atmospheric Chemistry and Physics: From Air Pollution to*
914 *Climate Change*, New York: John Wiley and Sons, 1998.

915 Sicard, M., C. Pérez, F. Rocadenbosch, J. Baldasano, and D. García-Vizcaino:
916 Mixed Layer Depth Determination in the Barcelona Coastal Area From Regular
917 Lidar Measurements: Methods, Results and Limitations. *Boundary Layer*
918 *Meteorology* 119, 135-157, 2006.

919 Sokół, P., I. Stachlewska, I. Ungureanu, and S. Stefan: Evaluation of the boundary
920 layer morning transition using the CL-31 ceilometer signals, *Acta Geophys.*,
921 62(2), doi:10.2478/s11600-013-0158-5, 2014.

922 Stull, R.: *An Introduction to Boundary Layer Meteorology*, Kluwer Academic
923 Publishers, Dordrecht, 1988.

924 Su, F., M. Yang, J. Zhong, Z. Zhang: The effects of synoptic type on regional
925 atmospheric contamination in North China, *Res. Of Environ. Sci.*, 17(3),
926 doi:10.13198/j.res.2004.03.18.sufq.006, 2004.

927 Tang, G., J. Zhang, X. Zhu, T. Song, C. Münkel, B. Hu, K. Schäfer, Z. Liu, J. Zhang,
928 L. Wang, J. Xin, P. Suppan, and Y. Wang: Mixing layer height and its
929 implications for air pollution over Beijing, China, *Atmos. Chem. Phys.*, 16(4),
930 2459-2475, doi:10.5194/acp-16-2459-2016, 2016.

931 Tang, G., P. Zhao, Y. Wang, W. Gao, M. Cheng, J. Xin, X. Li, Y. Wang: Mortality and
932 air pollution in Beijing: the long-term relationship. *Atmos. Environ.*, 150,
933 238-243, doi: 10.1016/j.atmosenv.2016.11.045, 2017a.

934 Tang, G., X. Li, Y. Wang, J. Xin, and X. Ren: Surface ozone trend details and
935 interpretations in Beijing, 2001-2006, *Atmos. Chem. Phys.*, 9, 8813-8823,

936 doi:10.5194/aep-9-8813-2009, 2009.

937 Tang, G., X. Zhu, B. Hu, J. Xin, L. Wang, C. Munkel, G. Mao, and Y. Wang: Impact

938 of emission controls on air quality in Beijing during APEC 2014: lidar ceilometer

939 observations, *Atmos. Chem. Phys.*, 15(21), 12667-12680,

940 doi:10.5194/aep-15-12667-2015, 2015.

941 Tang, G., X. Zhu, J. Xin, B. Hu, T. Song, Y. Sun, J. Zhang, L. Wang, M. Cheng, N.

942 Chao, L. Kong, X. Li, Y. Wang. Modelling study of boundary layer ozone over

943 northern China—Part I: Ozone budget in summer. *Atmos. Res.*, 187, 128-137,

944 2017b.

945 Tang, G., Y. Wang, X. Li, D. Ji, S. Hsu, and X. Gao: Spatial-temporal variations in

946 surface ozone in Northern China as observed during 2009–2010 and possible

947 implications for future air quality control strategies, *Atmos. Chem. Phys.*, 12,

948 2757-2776, doi:10.5194/aep-12-2757-2012, 2012.

949 Tomasi, F., M. Miglietta, and M. Perrone: The Growth of the Planetary Boundary

950 Layer at a Coastal Site: a Case Study, *Bound. Lay. Meteorol.*, 139:521-541, doi:

951 10.1007/s10546-011-9592-6, 2011.

952 Tu, J., S. Zhang, X. Cheng, W. Yang, and Y. Yang: Temporal and Spatial Variation of

953 Atmospheric Boundary Layer Height (ABLH) over the Yellow East China Sea, *J.*

954 *Ocean U. China*, 42(4):7-18, 2012.

955 Kamp, V., and I. McKendry: Diurnal and Seasonal Trends in Convective Mixed Layer

956 Heights Estimated from Two Years of Continuous Ceilometer Observations in

957 Vancouver, BC, *Bound. Lay. Meteorol.*, 137(3), 459-475,

958 doi:10.1007/s10546-010-9535-7, 2010.

959 Nair, V., K. Moorthy, D. Alappattu, P. Kunhikrishnan, S. George, P. Nair, S. Babu, B.

960 Abish, S. Satheesh, S. Tripathi, K. Niranjana, B. Madhavan, V. Srikant, C. Dutt, K.

961 Badarinarath, and R. Reddy: Wintertime aerosol characteristics over the

962 Indo-Gangetic Plain (IGP): Impacts of local boundary layer processes and

963 long-range transport, *J. Geo. Res.:* 2006JD008099, doi:10.1029/2006JD008099,

964 2007.

965 Wagner, M., S. Emeis, V. Freudenthaler, B. Heese, W. Junkermann, C. Munkel, K.

966 Schäfer, M. Seefeldner, and S. Vogt: Mixing layer height over Munich, Germany:

967 Variability and comparisons of different methodologies, *J. Geophys. Res.*, 111,

968 D13201, doi:10.1029/2005JD006593, 2006.

969 Wagner, P., and K. Schäfer: Influence of mixing layer height on air pollutant

970 concentrations in an urban street canyon, *Urban Climate*,

971 <http://dx.doi.org/10.1016/j.uclim.2015.11.001>, 2015.

972 Wang, L., N. Zhang, Z. Liu, Y. Sun, D. Ji, and Y. Wang: The Influence of Climate

973 Factors, Meteorological Conditions, and Boundary Layer Structure on Severe

974 Haze Pollution in the Beijing-Tianjin-Hebei Region during January 2013, *Adv.*

975 *Meteorol.*, 2014, 1-14, doi:10.1155/2014/685971, 2014.

976 Wang, Y., L. Yao, L. Wang, Z. Liu, D. Ji, G. Tang, J. Zhang, Y. Sun, B. Hu, and J. Xin:

977 Mechanism for the formation of the January 2013 heavy haze pollution episode

978 over central and eastern China, *Sci. China Earth Sci.*, 57(1), 14-25,

979 doi:10.1007/s11430-013-4773-4, 2013a.

980 Wang, Y., M. Zamora, and R. Zhang: New Directions: Light absorbing aerosols and
981 their atmospheric impacts, *Atmos. Environ.*, 81, 713-715, doi:
982 10.1016/j.atmosenv.2013.09.034, 2013b.

983 Wei, J., G. Tang, X. Zhu, L. Wang, Z. Liu, M. Cheng, C. Munkel, X. Li, and Y. Wang:
984 Thermal internal boundary layer and its effects on air pollutants during summer
985 in a coastal city in North China, *Journal of Environmental Sciences*, 1001-0742,
986 doi:10.1016/j.jes.2017.11.006, 2017.

987 Wiegner, M., F. Madonna, I. Biniotoglou, R. Forkel, J. Gasteiger, A. Geiß, G.
988 Pappalardo, K. Schäfer, and W. Thomas: What is the benefit of ceilometers for
989 aerosol remote sensing? An answer from ERALINET, *Atmos. Meas. Tech.*, 7,
990 1979-1997, doi: 10.5194/amt 7 1979 2014, 2014.

991 Xu, R., G. Tang, Y. Wang, and X. Tie: Analysis of a long-term measurement of air
992 pollutants (2007-2011) in North China Plain (NCP): Impact of emission
993 reduction during the Beijing Olympic Games, *Chemosphere*, 159, 647-658,
994 doi:10.1016/j.chemosphere.2016.06.025, 2016.

995 Yu, H., S. Liu, and R. Dickinson: Radiative effects of aerosols on the evolution of the
996 atmospheric boundary layer, *J. Geo. Res.: Atmos.*, 107, D12(4142),
997 doi:10.1029/2001JD000754, 2002.

998 Zhang, Z., X. Cai, Y. Song, L. Kang, X. Huang, and Q. Li: Temporal and spatial
999 variation of atmospheric boundary layer height over Hainan Island and its
1000 adjacent sea areas, *Acta. Sci. Nat. Univ. Pekin.*, 49:83-90, doi:
1001 10.13209/j.0479-8023.2013.105, 2013.

1002 Zhang, H., Y. Wang, J. Hu, Q. Ying, and X. Hu: Relationships between meteorological
1003 parameters and criteria air pollutants in three megacities in China, *Environ. Res.*,
1004 140, 242-254, doi:10.1016/j.envres.2015.04.004, 2015a.

1005 Zhang, J., Y. Sun, Z. Liu, D. Ji, B. Hu, Q. Liu, and Y. Wang: Characterization of
1006 submicron aerosols during a month of serious pollution in Beijing, 2013, *Atmos.*
1007 *Chem. Phys.*, 14(6), 2887-2903, doi:10.5194/acp-14-2887-2014, 2014.

1008 Zhang, Q., J. Xin, Y. Yin, L. Wang, and Y. Wang: The Variation and Trends of MODIS
1009 C5 & C6 Products' Errors in the Recent Decade over the Background and Urban
1010 Areas of North China, *Remote Sensing*, 8(9), 754, doi:10.3390/rs8090754,
1011 2016b.

1012 Zhang, R., G. Hui, S. Guo, M. Zamora, Q. Ying, Y. Lin, W. Wang, M. Hu, and Y.
1013 Wang: Formation of Urban Fine Particulate Matter, *Chem. Rev.*, 115, 3803-3855,
1014 doi: 10.1021/acs.chemrev.5b00067, 2015b.

1015 Zhang, R.: Getting to the Critical Nucleus of Aerosol Formation, *Science*, 328(5984),
1016 1366-1367, doi: 10.1126/science.1189732, 2010.

1017 Zhang, W., J. Guo, Y. Miao, H. Liu, Y. Zhang, Z. Li, and P. Zhai: Planetary boundary
1018 layer height from CALIOP compared to radiosonde over China, *Atmos. Chem.*
1019 *Phys.*, 16, 9951-9963, doi: 10.5194/acp-16-9951-2016, 2016a.

1020 Zhao, X., P. Zhao, J. Xu, W. Meng, W. Pu, F. Dong, D. He, and Q. Shi: Analysis of a
1021 winter regional haze event and its formation mechanism in the North China Plain,
1022 *Atmos. Chem. Phys.*, 13 (11), 5685-5696, 2013.

1023 Zhu, X., G. Tang, B. Hu, L. Wang, J. Xin, J. Zhang, Z. Liu, C. Munkel, and Y. Wang:

1024
1025
1026
1027
1028
1029
1030
1031
1032
1033
1034

~~Regional pollution and its formation mechanism over North China Plain: A case study with ceilometer observations and model simulations, J. Geo. Res.: Atmos., 2016JD025730, doi:10.1002/2016JD025730, 2016.~~